Angewandte Chemie
Eine Zeitschrift der Gesellschaft Deutscher Chemiker

Supporting Information

Multidirectional Activity Control of Cellular Processes by a Versatile Chemo-optogenetic Approach

*Xi Chen, Muthukumaran Venkatachalapathy, Leif Dehmelt, and Yao-Wen Wu**

anie_201806976_sm_miscellaneous_information.pdf
anie_201806976_sm_Movie_S1.avi
anie_201806976_sm_Movie_S2.avi
anie_201806976_sm_Movie_S3.avi
anie_201806976_sm_Movie_S4.avi
anie_201806976_sm_Movie_S5.avi

Supplementary Information

Table of Contents

METHODS AND MATERIALS:

Cloning

Fluorescent protein vectors were commercially available from Clontech. Fragments of interest were directly cut from the parent plasmids using appropriate restriction enzymes and gel purified using E.Z.N.A.® Gel Extraction Kit (OMEGA bio-tek, D2500-02) applying spin protocol, or amplified by PCR from plasmids containing the desired genes and purified by E.Z.N.A.® cycle pure kit (OMEGA Bio-tek, D6492-02) applying spin protocol. The purified gene inserts were first digested with appropriate restriction enzymes (FastDigest® enzymes from Thermo Scientific), purified by E.Z.N.A.® cycle pure kit as mentioned above, and then ligated using T4 DNA ligase (ThermoFisher Scientific, EL0011) into one of the fluorescent protein vectors or other appropriate parent vectors precut with the same restriction enzymes. Sometimes, pre-cut parent vectors were first dephosphorylated using FastAP Thermosensitive Alkaline Phosphatase (ThermoFisher Scientific, EF0654) prior to ligation in order to prohibit self-ligation of the linearized vector and to increase the subsequent ligation efficacy. Multiple fragments were assembled by stepwise cloning. The constructed plasmids were purified using QIAprep® Spin Miniprep Kit (QIAGEN, #27106) or E.Z.N.A. Plasmids DNA Mini it I (OMEGA Bio-tek, D6943-02) and were obtained at a concentration around 400-600 ng/µl. Parental plasmids encoding eDHFR, 2×FKBP', NLS (nucleus localization sequence) and Rac1Q61LΔCAAX (i.e. Rac1*) were described previously[1-3]. eDHFR gene was amplified using the forward primer: 5'- ATTTCCGGAGCTATGATCAGTCTGATTGC-3', and the reversed primer: 5'-AAACTCGAGCCGCCGCTCCAGAAT-3'). 2xFKBP' gene was amplified using the following forward primer: 5'-AAGTCCGGACTCAGATCTCG-3', and the reversed primer: 5'-ATTGCGGCCGCTTTAGTCGGATCCTTCCAGTTTTAG-3'. The parent plasmid encoding KIF5BN [i.e. KIF5B (1-560)] was obtained from pERB258 which was a gift from Michael Lampson (Addgene plasmid #67760). BicD2N [e.g. BicD2 (1-594)] gene was amplified from pBa-flag-BicD2 594-FKBP which was a gift from Gary Banker (Addgene plasmid # 64206)[4] (forward primer: 5'-AAAGGTACCTATCATGGATTACAAGGATGACGA-3'; reverse primer: 5'- AAAGGATCCCGATCTGCTCGGCCCA-3'). HaloTag gene was amplified from a HaloTag containing plasmid previous reported in our lab[2] (forward primer: 5'- AAGTCCGGACTCAGATCTATG-3'; reversed primer: 5'-ATTGCGGCCGCTTTAGGAAATCTCGAGCGTCGACA-3').

Cell culture and transfection

HeLa, COS-7, HEK 293T, MCF-7 and SH-SY5Y cells were cultured in minimum essential medium Eagle (MEME, # M4655, Sigma) solution supplemented with 8.8-10% FBS, 1% NEAA (non-essential aminoacids), 1% GlutMax, 1% penicillin-streptomycin and 1% sodium pyruvate at 37°C under 5% CO_2. For transfection, 5000-10000 cells were seeded in each well of an 8-well imaging tissue culture chamber (ibidi µ-Slide ibiTreat, or SARSTEDT x-well slide) prior to transfection using X-treme GENE HP DNA transfection reagent (REF: 06366236001, Roche). Dimerizer treatment and microscopic analysis were performed ~24h post transfection.

Microscopy and photo-uncaging

Confocal laser scanning microscopy (CLSM) was performed using the inverted confocal microscopes Zeiss LSM510 (EC Plan-NEOFLUAR, 40 x, oil, NA 1.3 objective) or Leica TCS SP5 AOBS (63×/1.4 HCX Plan Apo oil immersion objective), inside a temperature-controlled chamber at 37°C under 5 % CO_2. Cells were imaged in transparent full MEM (phenol red free, REF: 51200-046, Life technologies) or full DMEM (phenol red free, Life technologies, REF: 21063-29) supplemented with additional 8.8-10% FBS, 1% sodium pyruvate, 1% NEAA and 1% penicillin-streptomycin. For introducing caged TMP to HaloTag, cells were treated with NvocTMP-Cl (5 µM, 1h), rinsed (3 × PBS), incubated in imaging medium for 30 min, and rinsed again (2 × PBS) before imaging. Perturbations by photo-uncaging were performed on a Zeiss LSM 510 microscope equipped with a 40× oil objective or on a Leica SP5 microscope equipped with a 63x oil objective using 405 nm lasers with illumination doses of 3 - 6 $J \cdot cm^{-2}$ that triggers the maximal degree of dimerization. The illumination dose was calculated using the following formula:

Illumination dose = [laser power × pixel dwell time]/pixel area

In a typical experiment using the Zeiss LSM510 microscope, photo-uncaging was performed using a 405 nm laser with ~200 µW power (@ 100% power), scanning with a pixel dwell time of 3.2 µs in a 512 pixel × 512 pixel image [64 µm × 64 µm, 3.5× zoom in] that gives a pixel area of 0.016 μm^2, resulting in an illumination dose of: (200 µW × 3.2 µs)/0.016 μm^2 = 4 $J \cdot cm^{-2}$.

On the Leica SP5 microscope, photo-uncaging was typically performed using ~180 µW laser power (@ 100% power) by scanning the imaging field once at a speed of 400 Hz (ca. pixel dwell time of 4.88 µs) in a 512 pixel × 512 pixel image [61.5 µm × 61.5 µm, 4× zoom in] that gives a pixel area of 0.00144 μm^2, resulting in an illumination dose of: (180 µW × 4.88 µs)/0.0144 μm^2 = 6 $J \cdot cm^{-2}$.

Different illumination doses were achieved by varying the pixel dwell time via scan speed settings or by adjusting the 405 nm laser power intensity. Laser power intensities were measured at the objective using *Field MaxII-TOP laser power and energy meter* from Coherent.

Image analysis and data regression

Microscopic images were analyzed and processed with ImageJ (NIH, Bethesda) and prepared for presentation using Microsoft PowerPoint. Image manipulations were restricted to adjustment of brightness levels, cropping, background subtraction, scaling and false color-coding using LUTs. Pearson's correlation coefficient (PCC) was employed for colocalization analysis using the "Manders_Coefficients.class" plugin for Image-J (http://wwwfacilities.uhnresearch.ca/wcif/software/Plugins/Manders_Coefficients.html) with the images set at 8 bit. Sigma-Plot and Microsoft Excel were used for plotting, data fitting and statistical analysis. Unless stated otherwise in the corresponding figure legends, sample size for microscopy-based analyses was based on performing at least three independent biological replications. Measurements from all experimental manipulations were included in the statistical analyses, unless stated otherwise. Student's *t*-tests were used to compare two experimental conditions. In most cases, paired *t*-tests were performed, in which measurements were linked, as for example concerning pre- versus post-uncaging conditions for the same cell. Otherwise, unpaired tests were used. Stars denote P-values for indicated statistical tests (*: P<0.05, **: P<0.01, ***: P<0.001; ****: P<0.0001, n.s.: not significant).

Procedures for multi-directional activity control:

In the "parallel MAC" approach, after the treatment of NvocTMP-Cl (5 µM, 1h, then washed), 0.3 µM of SLF'-TMP was added to the cell culture medium for 15 min. The medium was briefly washed by PBS, then replaced by clear MEM or DMEM lacking phenol-red and incubated for 5 min to remove excess of SLF'-TMP before photo-activation.

In the "competitive MAC" approach on protein positioning, after the treatment of NvocTMP-Cl (5 µM, 1h, then washed), the cells were illuminated with a 405 nm laser, leading to translocation of a POI (e.g. Rac1) from the first location (e.g. cytosol) to the second location (e.g. PM or mitochondria); after the treatment of SLF*-TMP (10 or 15 µM), the POI was rerouted from the second position (e.g. PM or mitochondria) to the third location (e.g. nucleus); and after briefly rinse the cell (1×PBS), the addition of TMP (10 µM) led to

the translocation of the POI from the third location (e.g. nucleus) back to the cytosol (the initial location). Additional rounds are possible by applying further TMP wash-out (3×PBS) and S*T addition.

In the “competitive MAC” approach on organelle positioning, the cells were pre-treated with NvocTMP-Cl (5 µM, 1h, then washed). Subsequently, cells were illuminated with a 405 nm laser to allow recruitment of the first microtubule motor activity to peroxisomes. 4-10min post photoactivation (denoted as “post PA” in respective figures and figure legends), SLF*-TMP (10 µM) was added to replace the motor activity on peroxisomes. 5-10min later after the addition of SLF*-TMP (denoted as “post S*T” in respective figures and figure legends), TMP (10 µM) was added to release the exchanged motor activity from peroxisomes and to stop the transport of peroxisomes.

SUPPLEMENTARY SCHEMES AND FIGURES

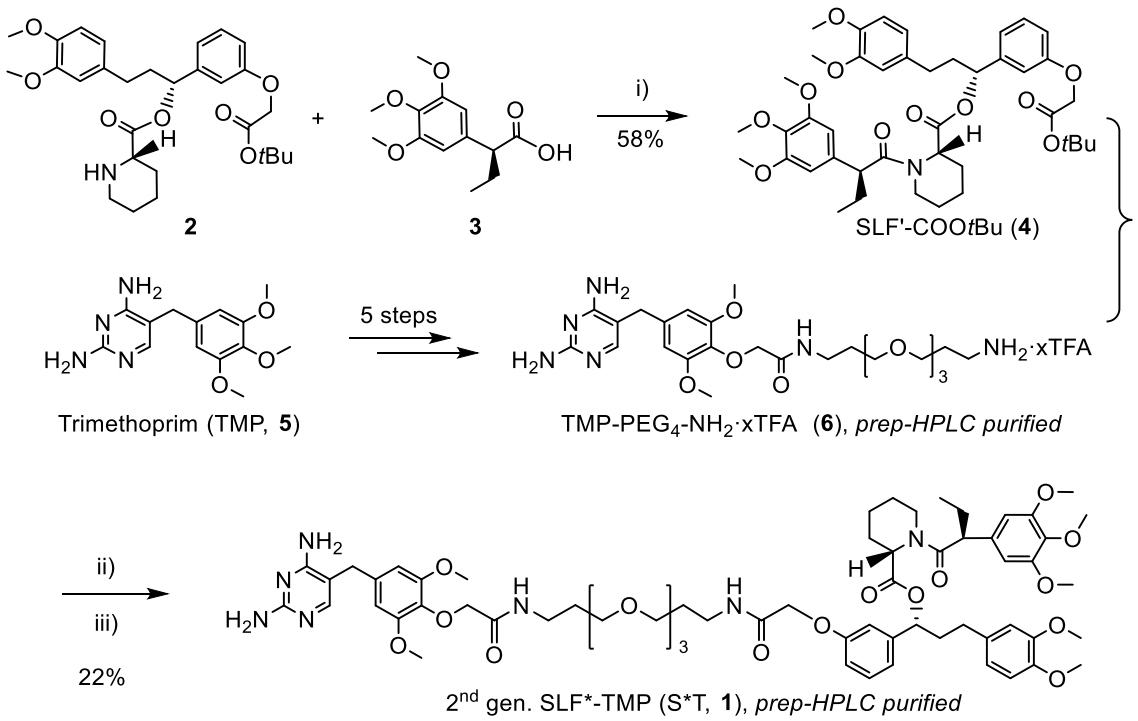

Scheme S1. Synthesis of the 2nd gen. SLF*-TMP (S*T, 1). i) EDC·HCl, HOBt·H_2O, DIEA, DCM, room temperature (RT), 1 day, 58% yield. ii) 50% TFA in DCM, overnight. iii) HATU, HOBt·H_2O, DIEA, DMF, RT, 8h, 22% yield from SLF'-COO*t*Bu (**4**). EDC: ethyl dimethylaminopropyl carbodiimide; HOBt·H_2O: 1-hydroxybenzotriazole hydrate; DIEA: *N*,*N*-diisopropylethylamine; DCM: dichloromethane; HATU: 1-[Bis(dimethylamino)methylene]-1H-1,2,3-triazolo[4,5-b]pyridinium 3-oxide hexafluorophosphate; DMF: dimethylformamide; TFA: trifluoroacetic acid.

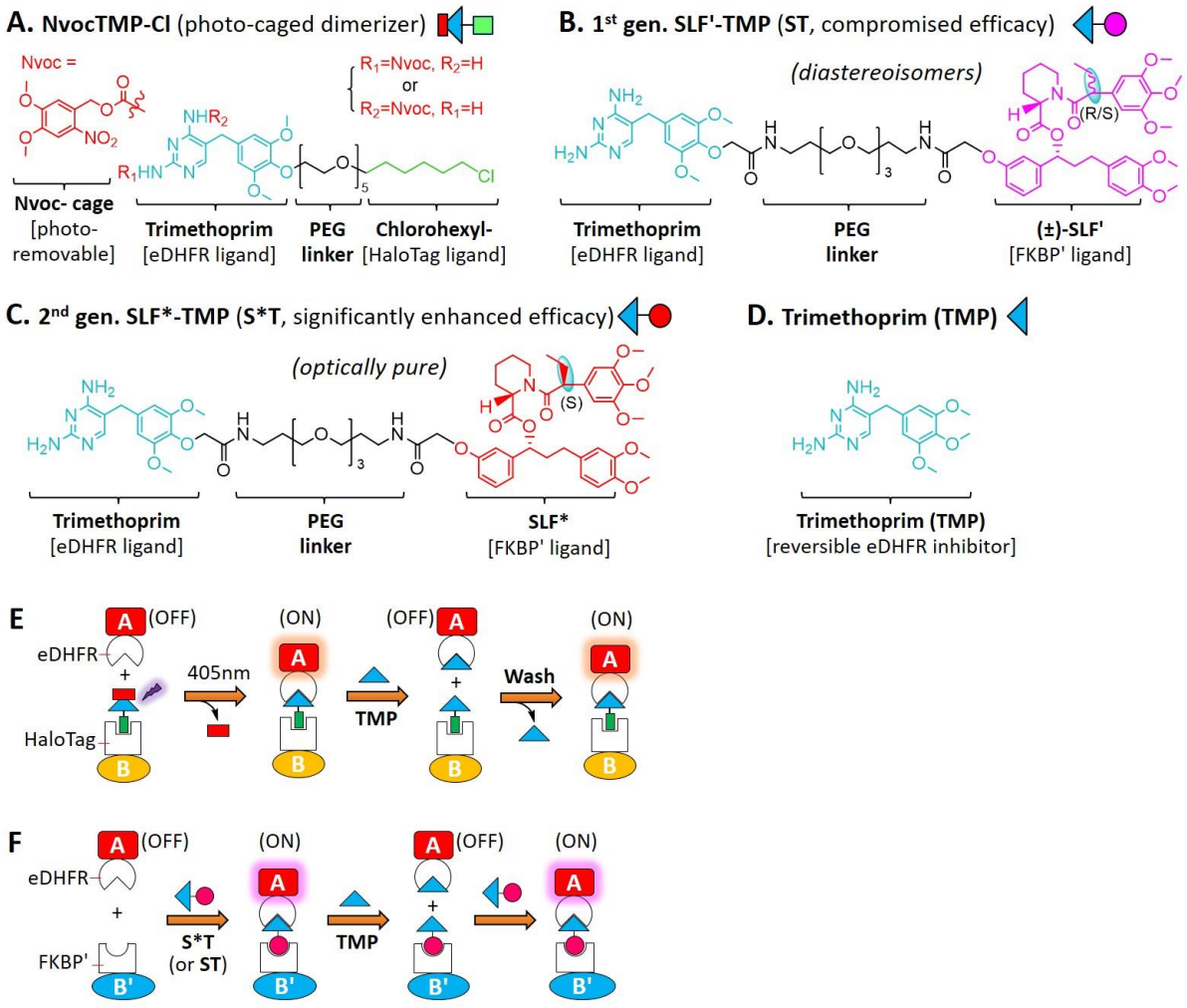

Figure S1. A-D) The three chemical dimerizers (NvocTMP-Cl, SLF*-TMP and SLF'-TMP) and competitor, trimethoprim (TMP), used in this study. NvocTMP-Cl consists of a caged trimethoprim (TMP), a HaloTag ligand (chlorohexyl group) and a polyethylene glycol (PEG) linker. TMP selectively binds to *E.coli* dihydrofolate reductase (eDHFR) and the chlorohexyl moiety can form a covalent bond with a bacterial alkyl dehalogenase mutant (HaloTag). The 1st gen. SLF'-TMP (ST) dimerizer is a diastereomeric mixture (R/S) with intermediate efficacy while the 2nd gen. SLF*-TMP (S*T) is optically pure (S) with a significantly enhanced efficacy. Trimethoprim (TMP) is a competitor that can disrupt the dimerization. **E**) Local illumination (e.g. 405 nm light) induces eDHFR recruitment to the HaloTag fusion and the addition of TMP reverses the dimerization process. By sequential application of TMP and wash-out, multiple rounds of reversible dimerization can be achieved. **F**) SLF*-TMP or SLF'-TMP features a TMP ligand and a SLF* [or (±)-SLF'] ligand which allows the dimerization between eDHFR and FKBP'; typically a fusion contains two copies of FKBP' (i.e. 2xFKBP') is used. By sequentially applying ST/S*T and TMP, multiple rounds of reversible dimerization can be achieved.

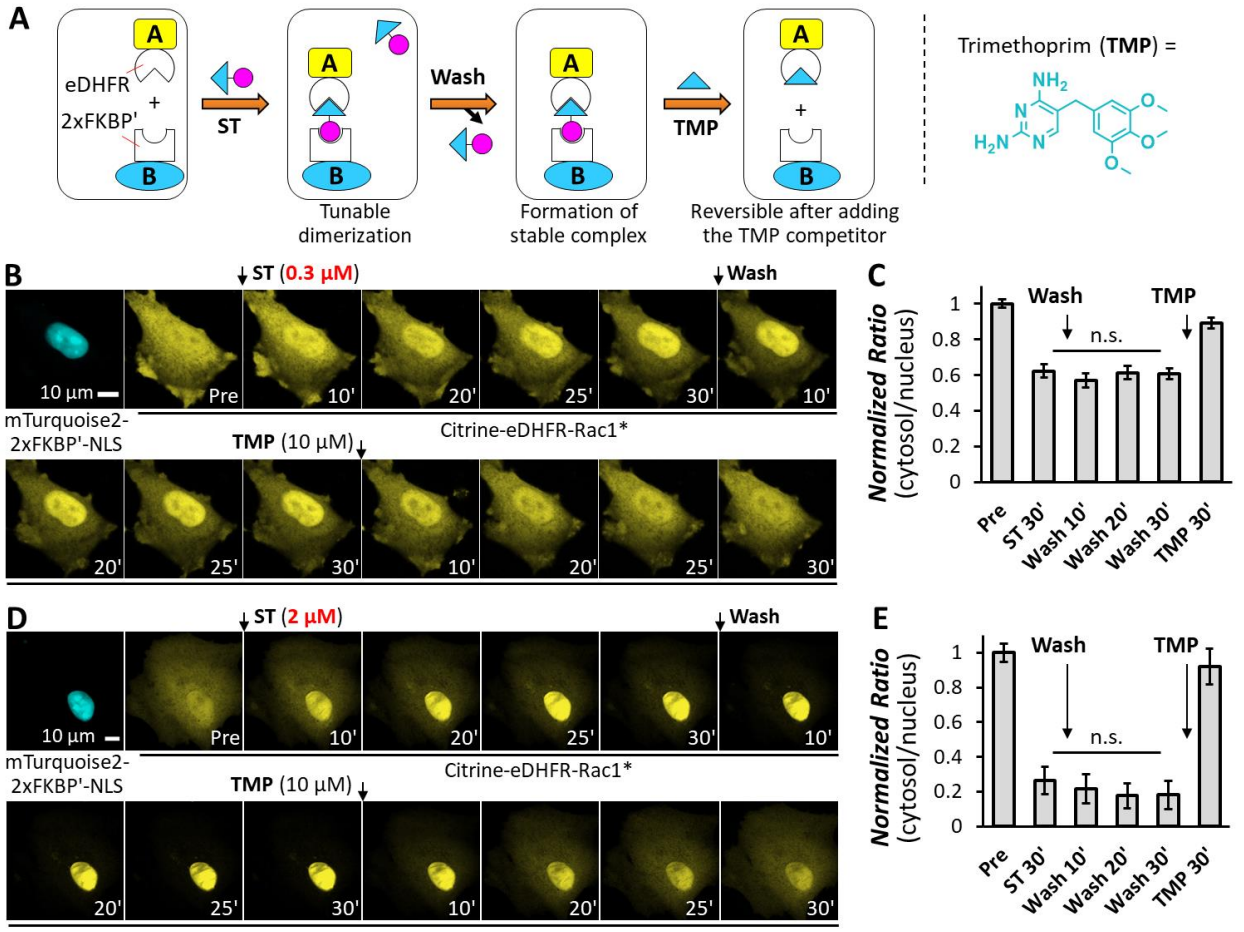

Figure S2. ST stably controls the cytosolic level of POI inside the cell. A) Schematic view of the experiment. **B**) The addition of 0.3 µM ST partially reduces the cytosolic Rac1* level and the recruitment of Rac1* into the nucleus that is stable after wash-out of ST; Rac1* can return to the cytosol after adding TMP (10 µM). **C**) Statistic analysis of the cytosolic level of Rac1 (cytosol/nucleus) after adding ST (0.3 µM), after wash-out of ST, and after the addition of TMP; n = 6 cells. **D**) The addition of 2 µM ST reduces the cytosolic level of Rac1* at a higher degree and the recruitment of Rac1* into the nucleus is stable after wash-out of ST; Rac1* can return to cytosol after adding TMP (10 µM). **E**) Statistic analysis of the relative cytosolic level of Rac1 (cytosol/nucleus) after adding ST (2 µM), after wash-out of ST, and after the addition of TMP; n = 3 cells. Scale bars: 10 µm; error bars, standard error of the mean (SEM).

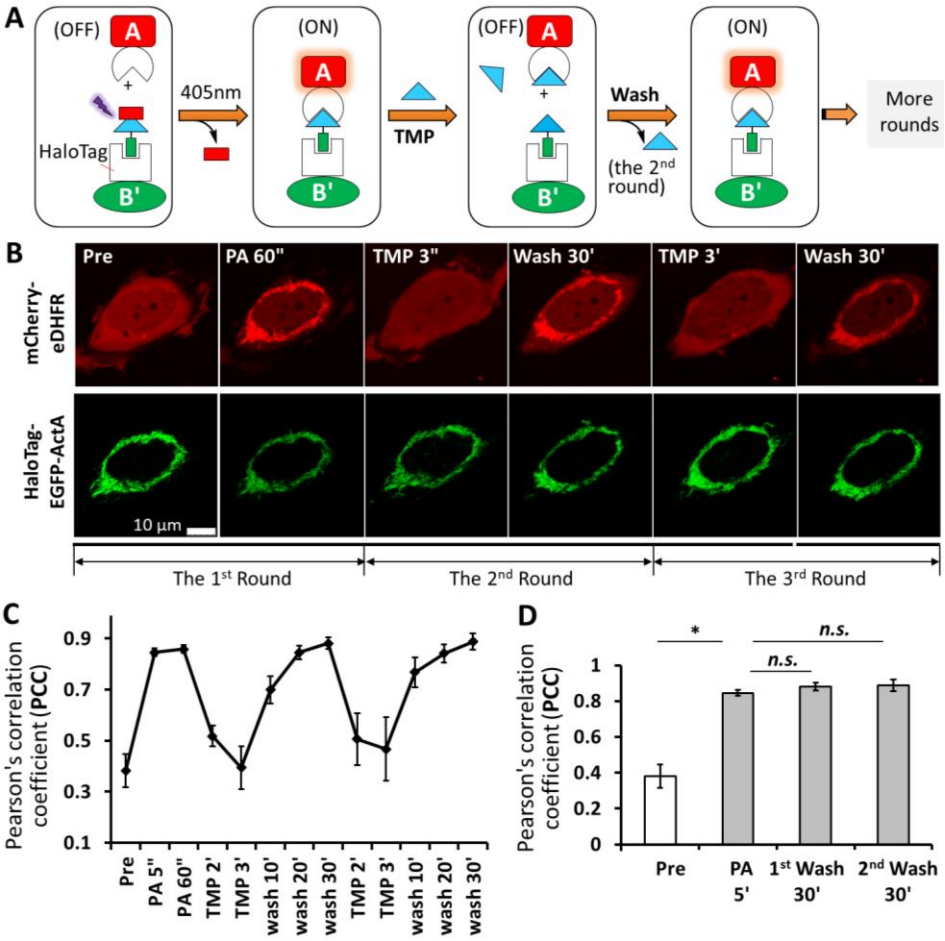

Figure S3. Multi-round reversibility of the NvocTMP-Cl dimerization system. A) Schematic view. The photo-caged NvocTMP-Cl dimerizer induces the dimerization between eDHFR and HaloTag fusions upon 405 nm laser illumination; multi-round of reversible dimerization is achieved by sequentially applying TMP and wash-out. **B**) Representative CLSM images of a HeLa cell co-expressing mCherry-eDHFR (red, cytosol) and HaloTag-EGFP-ActA (green, mitochondria). The cytosolic mCherry-eDHFR was recruited to mitochondria after photoactivation (PA 60"). The addition of the TMP competitor (5 µM) for 2-3 minutes reversed mCherry-eDHFR back to the cytosol (TMP 3'). After 30 minutes following competitor wash-out, a second recruitment of mCherry-eDHFR to mitochondria was observed (wash 30'). In addition, a third round of reversible dimerization was facilely achieved simply by repeating TMP competitor addition and wash-out. Scale bar: 10 µm. **C**) Pearson's correlation coefficient (PCC) analysis of the colocalization between mCherry-eDHFR and HaloTag-EGFP-ActA demonstrates multi-round and reversible protein dimerization. **D**) Paired Student's *t*-tests show that the dimerization degree does not decrease after the multi-round dimerization cycles. *: $p < 0.05$, *n.s.*: non-significant. For **C**) and **D**), n = 4 cells; error bars, SEM.

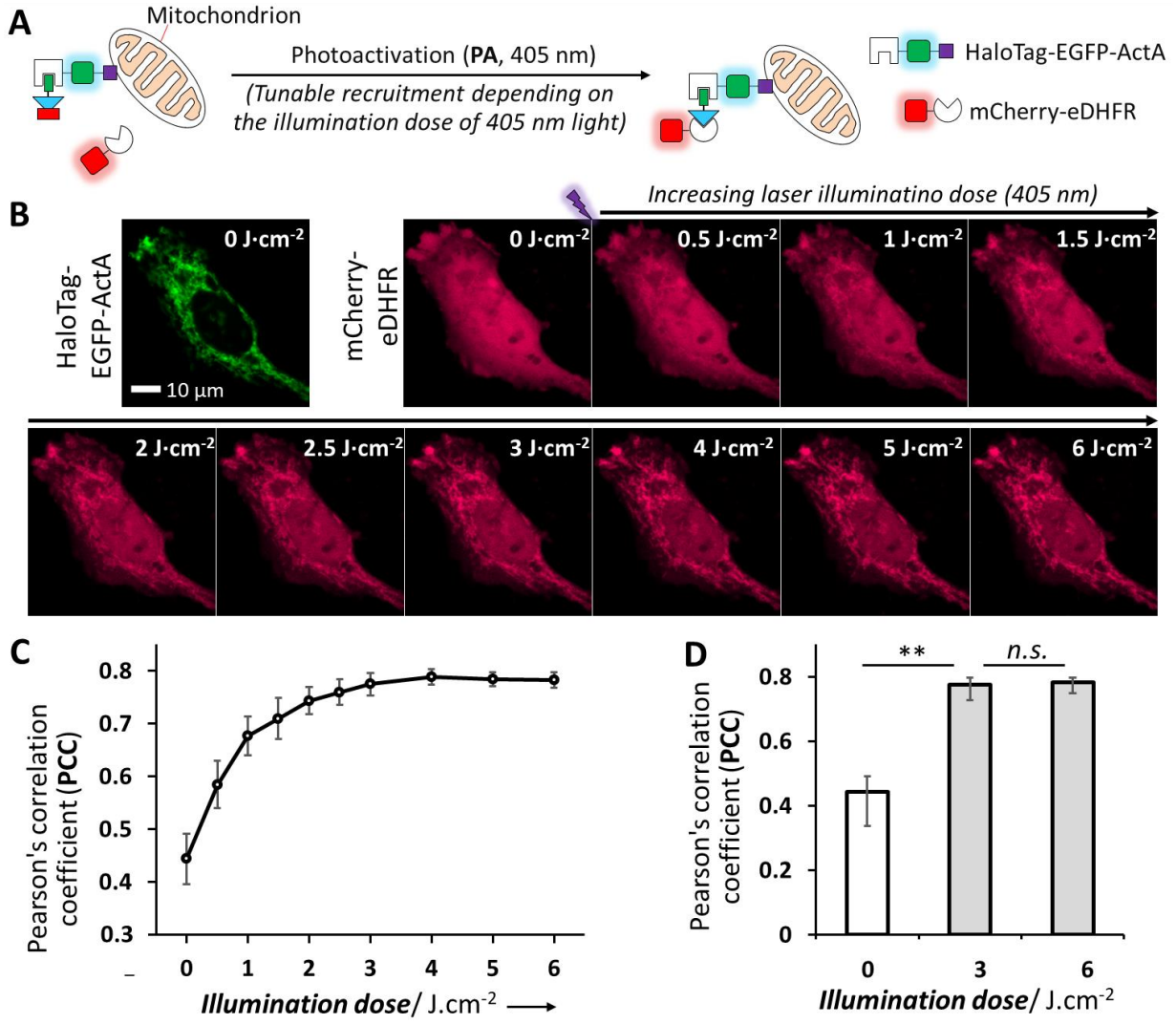

Figure S4. The degree of dimerization induced by NvocTMP-Cl is fine-tuned by light. A) Schematic view and the constructs used. **B**) A representative HeLa cell co-expressing mCherry-eDHFR (cytosol) and HaloTag-EGFP-ActA (mitochondria). Increasing doses of light illumination were titrated, resulting in dose-dependent targeting of cytosolic mCherry-eDHFR to mitochondria. An illumination dose (405 nm) of 3 J·cm^{-2} is sufficient to achieve almost the maximal degree of dimerization; ActA: the mitochondria targeting sequence of the *Listeria ActA* protein. Scale bar: 10 µm. **C**) The colocalization degree between mCherry-eDHFR and HaloTag-EGFP-ActA was analyzed by Pearson's correlation coefficient (PCC), which was plotted against the 405 nm laser illumination doses. **D**) Paired Student's *t*-test shows a significant increase of colocalization after 3 J·cm^{-2} of light illumination. Additional doses of illumination did not increase targeting. For **C**) and **D**) n=5 cells; error bars, SEM.

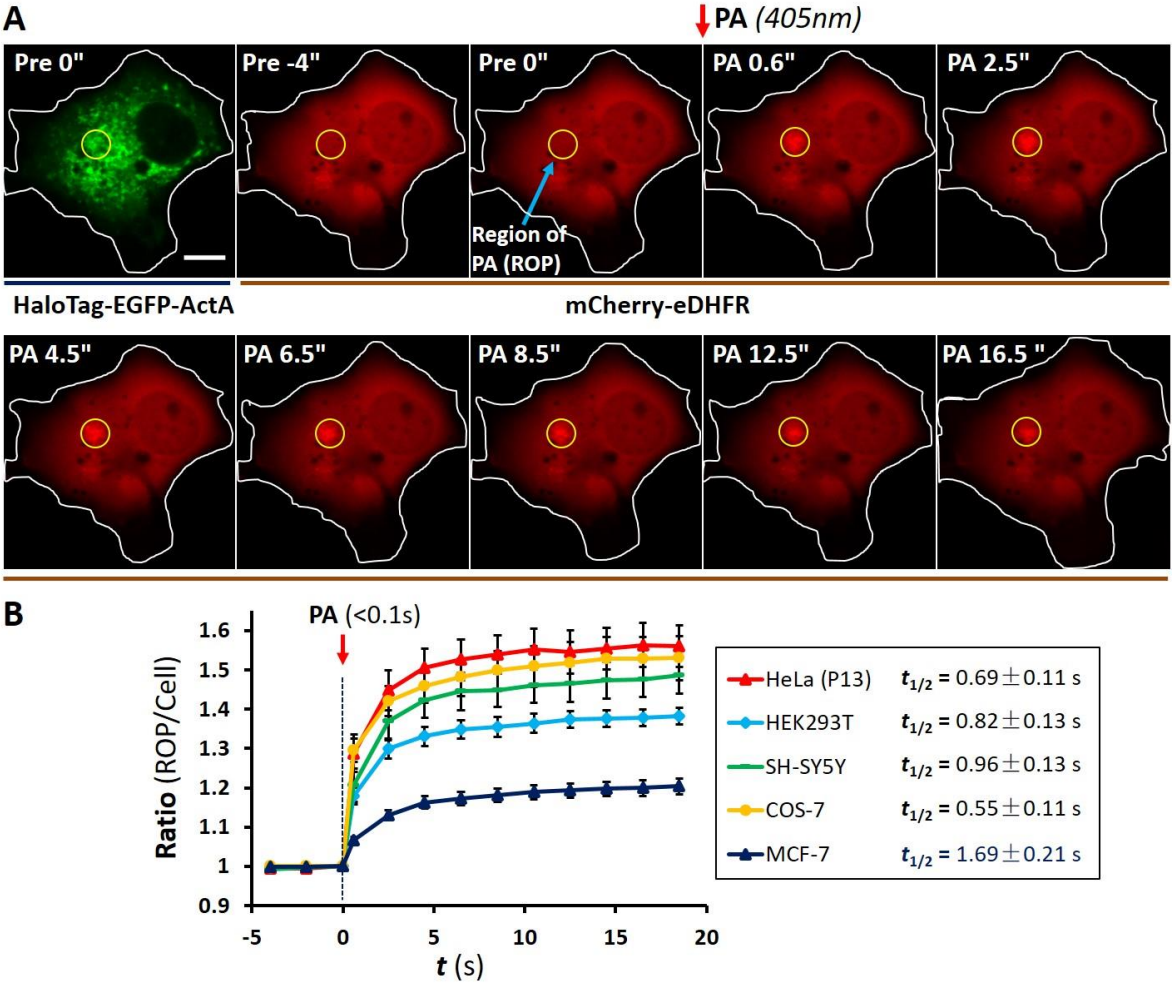

Figure S5. NvocTMP-Cl based dimerization is rapid and is generally applicable in various cell lines. HeLa, HEK293T, SH-SY5Y, COS-7, Neuro-2a, and MCF-7 were tested. **A**) Time series of a typical COS-7 cell co-expressing mCherry-eDHFR and HaloTag-EGFP-ActA before photoactivation (Pre -4" and Pre 0") and after local photoactivation (PA 0.6", PA 2.5", PA 4.5", PA 6.5", PA 8.5", PA 12.5" and PA 16.5") in the region of photoactivation (ROP). Scale bar: 10 µm. **B**) Normalized fluorescence intensity ratios of mCherry in the ROP versus the entire cell in different cell lines were plotted against time. Mono-exponential fitting led to half-time of light-induced dimerization ($t_{1/2}$). n = 6-11 cells of each cell lines were analyzed; error bars, SEM.

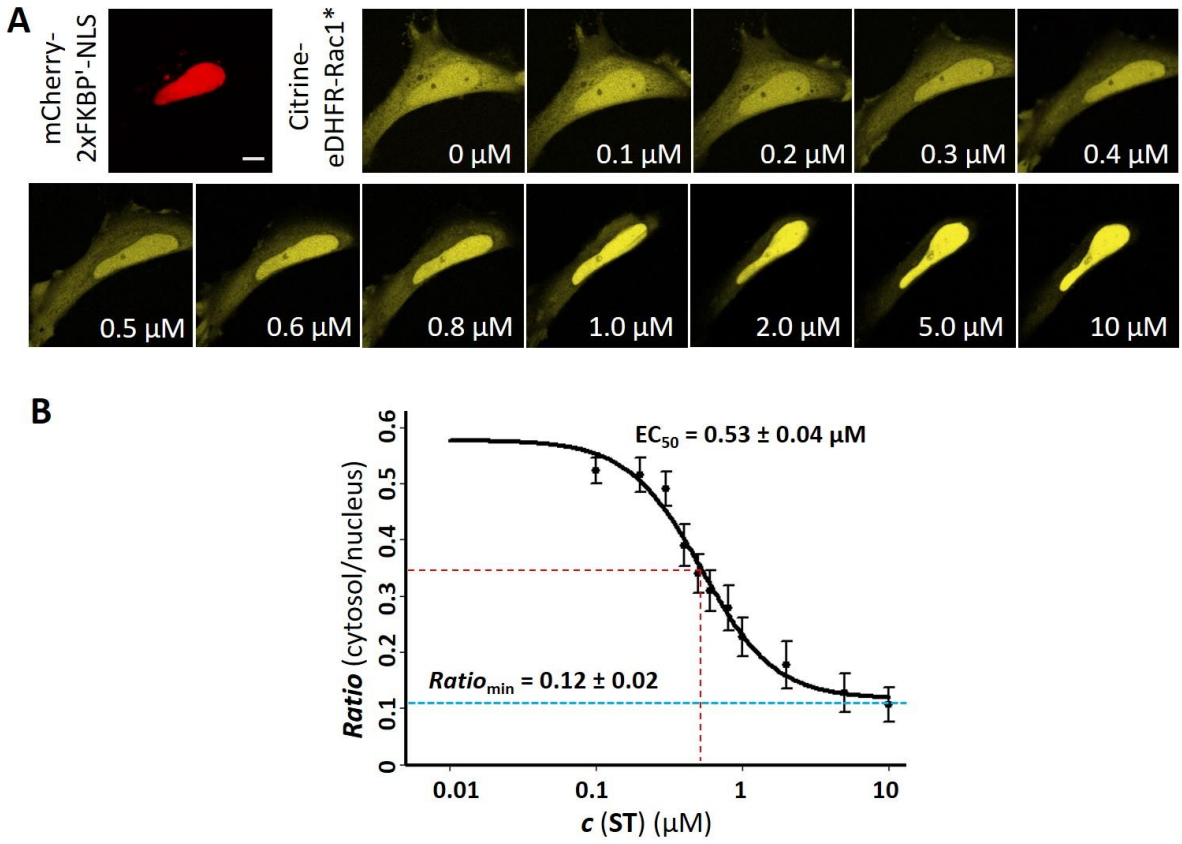

Figure S6. ST enables fine-tuning of the cytosolic Rac1* levels. **A**) HeLa cells co-expressing Citrine-eDHFR-Rac1* (cytosolic) and mCherry-2xFKBP'-NLS (nucleus) were titrated with increasing concentrations of ST. Representative confocal images reveal that the cytosolic protein level of Citrine-eDHFR-Rac1* can be fine-tuned by applying different concentrations of the ST dimerizer. Scale bar: 10 µm. **B**) Titration of ST reveals a dose-dependent decrease of the cytosol/nucleus ratio of the Citrine intensity with a half maximal effective concentration of EC_{50} = 0.53±0.04 µM (mean±s.d.) by fitting the data to the 4-parameter logistic (4PL) curve. This curve reveals a **cooperative binding model of ST induced dimerization**, where the addition of more ST does not inhibit the dimerization. The minimal Citrine intensity ratio between cytosol and nucleus (***Ratio***$_{min}$) is 0.12 ±0.02 (mean±s.d.), which is a reflection of the maximal dimerization degree that can be induced by ST. Mean values and SEM were shown; n=4 cells.

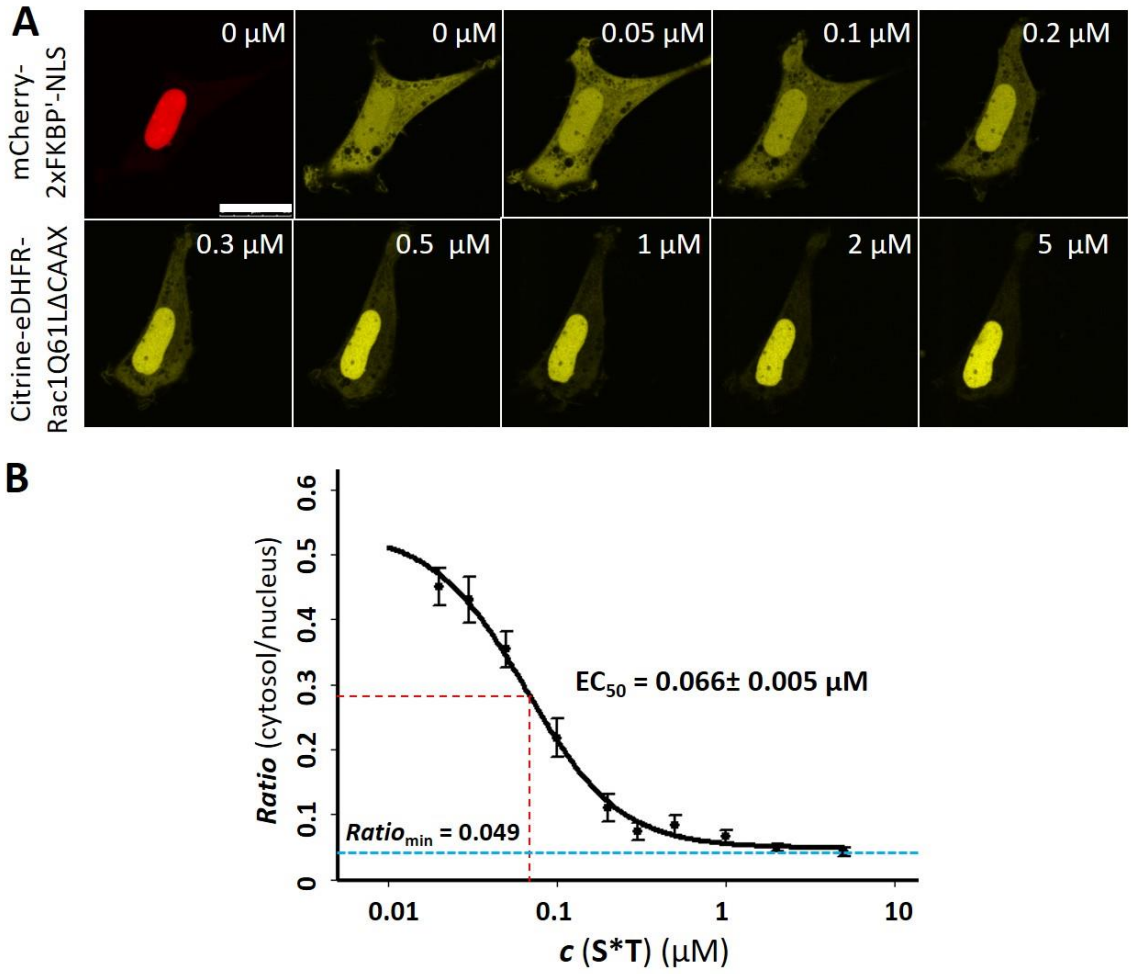

Figure S7. The optically pure 2nd gen. SLF*-TMP (S*T) shows a significantly enhanced efficacy in inducing the dimerization of FKBP'- and eDHFR-fused proteins, with a half maximal effective concentration EC_{50} = 0.066±0.005 µM (mean±s.d.) that is over eight times lower than that of SLF'-TMP (EC_{50} = 0.53 ± 0.04 µM). In addition, SLF*-TMP can induce dimerization with a higher degree [$\boldsymbol{Ratio}_{min}$ (cytosol/nucleus) = 0.049±0.008 (mean±s.d.)] than SLF'-TMP [$\boldsymbol{Ratio}_{min}$ (cytosol/nucleus) = 0.12±0.02 (mean±s.d.)]. **A)** A representative HeLa cell co-expressing mCherry-2xFKBP'-NLS (red channel, nucleus) and Citrine-eDHFR-Rac1Q61LΔCAAX (yellow channel, whole cell) was treated with increasing concentrations of SLF*-TMP. This led to a dose-dependent recruitment of Citrine-eDHFR-Rac1Q61LΔCAAX from the cytosol to the nucleus. Scale bar: 25 µm. NLS: nucleus localization signal. **B)** The intensity ratios (cytosol/nucleus) of Citrine was plotted against the concentrations of SLF*-TMP. The data were fitted to the 4PL curve to derive the EC_{50} value and the minimal Citrine intensity ratio ($\boldsymbol{Ratio}_{min}$). This curve reveals a **cooperative binding model of S*T induced dimerization**. n=10 cells; error bars, SEM.

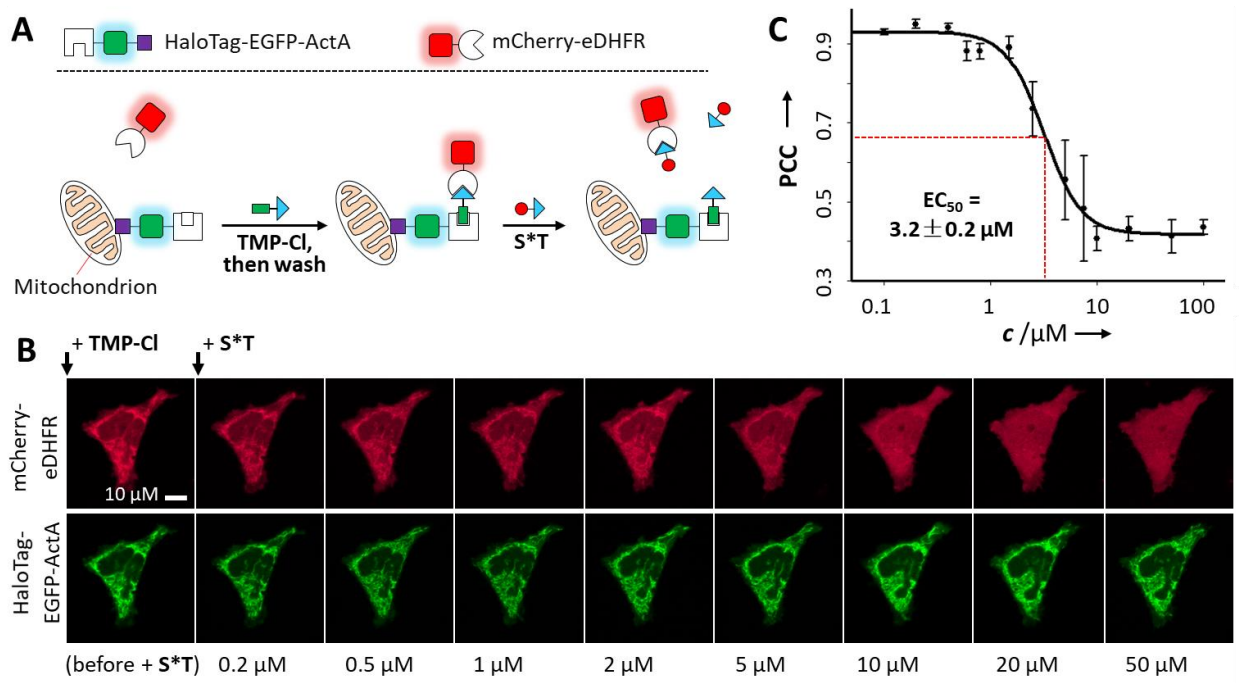

Figure S8. SLF*-TMP (S*T) competitively disrupts the dimerization between eDHFR and HaloTag that was initially induced by TMP-Cl (the uncaged form of NvocTMP-Cl). A) Constructs and the assay. **B**) A representative HeLa cell co-expressing mCherry-eDHFR (cytosol, upper channel) and HaloTag-EGFP-ActA (mitochondria, lower channel). TMP-Cl induces translocation of mCherry-eDHFR to mitochondria. The titration of increasing concentrations of S*T dimerizer gradually disrupts the dimerization. For each titration, images were taken 10-15min after the addition of S*T to ensure that saturated dimerization has reached. Scale bar: 10 µm. **C**) S*T inhibits the dimerization initially induced by TMP-Cl with an EC_{50} of 3.2±0.2 µM (mean±s.d.). The data were fitted to the 4PL curve. n=6 cells. PCC: Pearson's correlation coefficient between mCherry-eDHFR and HaloTag-EGFP-ActA; error bars, SEM.

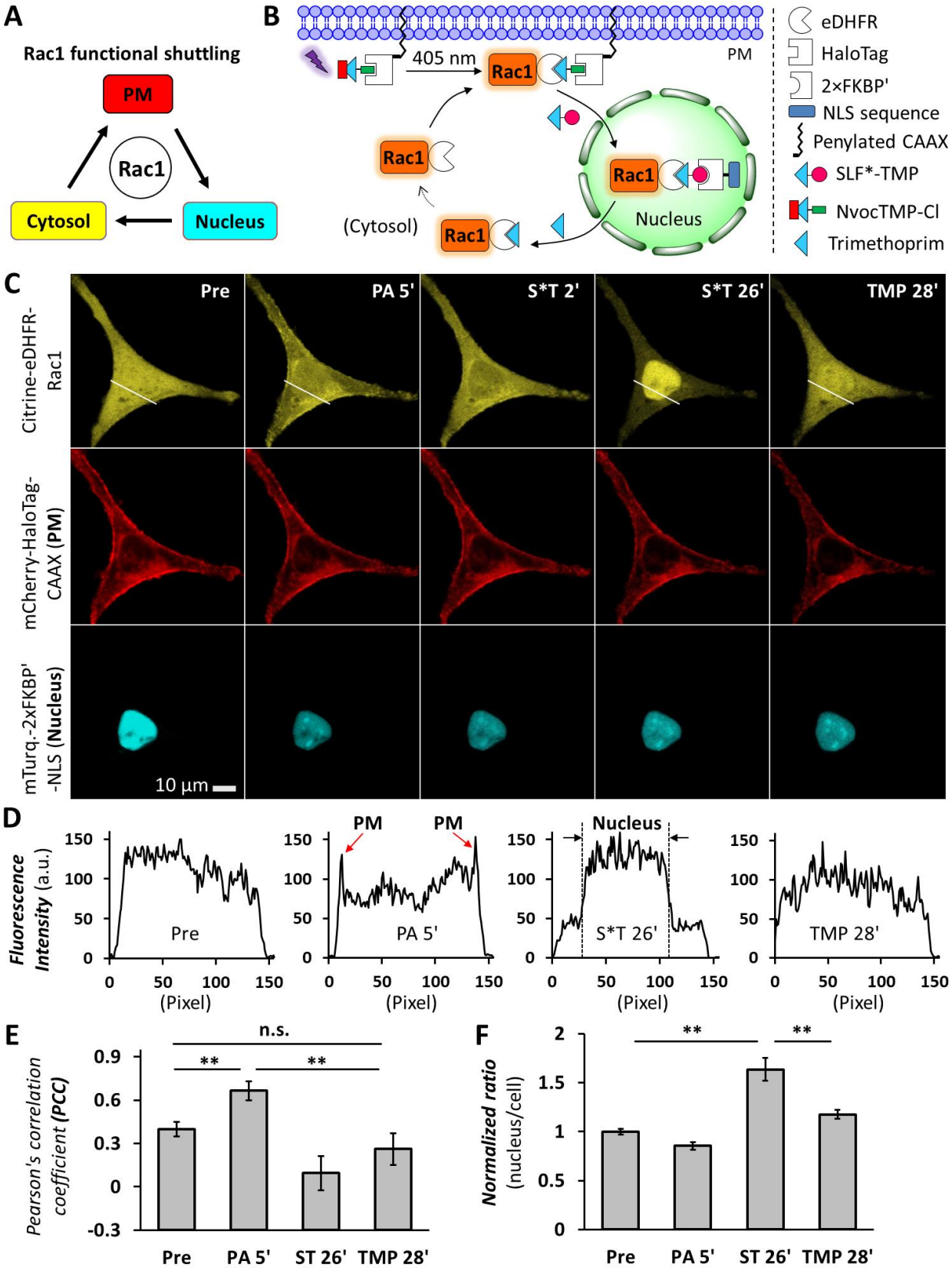
A
Rac1 functional shuttling
PM
Rac1
Cytosol
Nucleus
B
405 nm
PM
Rac1
(Cytosol)
Nucleus
eDHFR
HaloTag
2×FKBP'
NLS sequence
Penylated CAAX
SLF*-TMP
NvocTMP-Cl
Trimethoprim
C
Pre
PA 5'
S*T 2'
S*T 26'
TMP 28'
Citrine-eDHFR-Rac1
mCherry-HaloTag-CAAX (PM)
mTurq.-2xFKBP'-NLS (Nucleus)
10 µm
D
Fluorescence Intensity (a.u.)
PM
Nucleus
(Pixel)
E
n.s.
**
Pearson's correlation coefficient (PCC)
Pre
PA 5'
ST 26'
TMP 28'
F
Normalized ratio (nucleus/cell)

Figure S9. Multi-directional activity control (MAC) of Rac1 positioning inside a live cell. A). The nucleocytoplasmic shuttling of Rac1 plays an important role in cell invasiveness. **B**). Schematic view of the experiment and the denotation of the symbols used in the scheme. Illumination at 405 nm removes Nvoc group to expose active TMP moiety at the plasma membrane, leading to the recruitment of eDHFR-Rac1 from the cytosol to the plasma membrane; the addition of SLF*-TMP (S*T) dissociates eDHFR-Rac1 from the plasma membrane and then re-directs Rac1 to the nucleus; the addition of TMP disrupts the S*T-mediated dimerization and thus Rac1 returns to the cytosol. NLS: nucleus localization signal. **C**). Citrine-eDHFR-Rac1 (the protein of interest, at the cytosol, yellow), mCherry-HaloTag-CAAX (at the plasma membrane, red) and mTurquoise (at the nucleus, cyan) were co-expressed in HeLa cell. Rac1 distributed throughout the cell before photoactivation (Pre), was targeted to the plasma membrane after photoactivation (PA 5', 5 min after photoactivation), translocated to the nucleus after adding SLF*-TMP (S*T 2', S*T 26'), and finally returned to the cytosol after adding TMP (TMP 28'). Thus, a full cycle of Rac1 was achieved by manipulating Rac1 positioning among three different locations inside a cell. Scale bar: 10 μm. **D**). Line profile analysis (the white line in **C**) of the Rac1 images. a.u.: Arbitrary unit. **E**). Statistical analysis of the recruitment and dissociation of Rac1 at the plasma membrane using PCC colocalization analysis (Citrine and mCherry channels) at time points before PA (Pre), 5 min after PA (PA 5'), 26 min after the addition of S*T (S*T 26') and 28 min after the addition of TMP (TMP 28'). **F**) Statistical analysis of the recruitment and release of Rac1 inside the nucleus using the Citrine intensity ratio between nucleus and the entire cell at time points before PA (Pre), 5 min after PA (PA 5'), 26 min after the addition of S*T (S*T 26') and 28 min after the addition of TMP (TMP 28'). For **E**) and **F**), n = 5 cells; error bars, SEM.

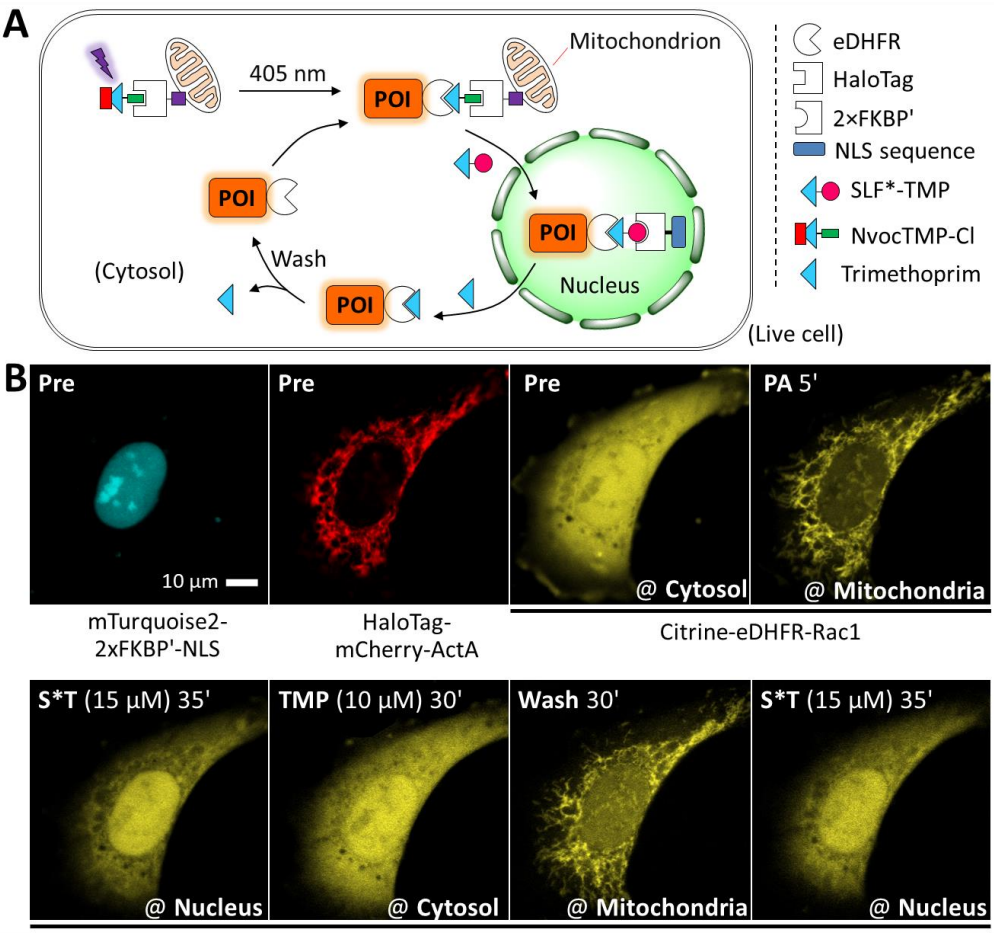

Figure S10. Competitive multi-directional activity control (MAC) can be operated in a cycling manner. A) Schematic view and symbols. **B**) Representative CLSM images of a live HeLa cell co-expressing mTurquoise2-2xFKBP'-NLS (nucleus, cyan), HaloTag-mCherry-ActA (red, mitochondria), and Citrine-eDHFR-Rac1* (yellow, entire cell) during the course of reversible MAC. Photoactivation (PA) using 405 nm laser targeted Rac1 protein in the entire cell (yellow) to mitochondria; the addition of S*T (15 µM) translocated Rac1 from mitochondria to the nucleus; after the addition of TMP (10 µM), Rac1 is restored in the cytosol; wash-out of TMP rerouted Rac1 to mitochondria in a second round and the addition of S*T (15 µM) for the second time targeted Rac1 into the nucleus again. Scale bar: 10 µm.

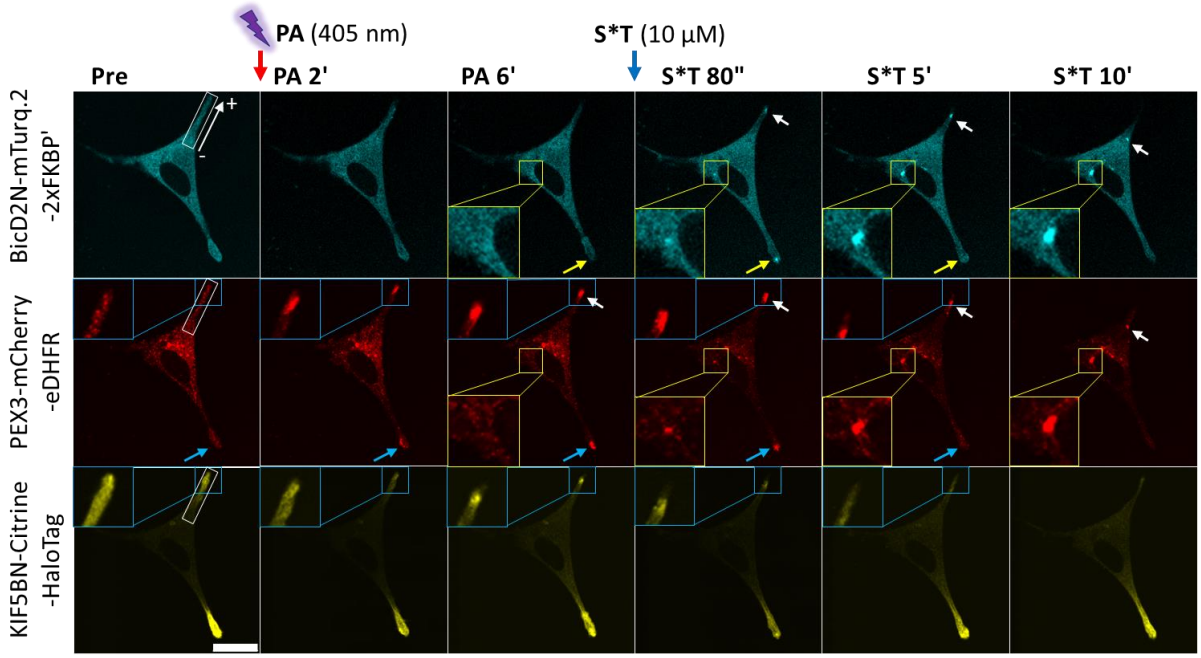

Figure S11. Competitive multi-directional activity control ("competitive MAC") of peroxisome transport. A cell protruding region at the cell periphery is highlighted by a white rectangular box. A time series of montages of the enlarged region labeled with the rectangular white box is shown in Figure 2F. Before photoactivation (PA), peroxisomes were dispersed throughout the cell (Pre). 2 min and 6 min after PA (PA 2' and PA 6', respectively), KIF5BN was recruited to peroxisomes (Citrine channel), which induced anterograde transport of peroxisomes to the cell periphery. In that region, clusters of peroxisomes formed (mCherry channel, highlighted in the enlarged blue squared region and indicated by arrows). After addition of S*T (10 µM), KIF5BN was released from peroxisomes (S*T 80", S*T 5', Citrine channel), along with the recruitment of BicD2N (S*T 80", S*T 5', mTurquoise channel). This induced the retrograde transport of the peroxisomes to the cell center (S*T 80" → S*T 5' → S*T 10", mTurquoise2 and mCherry channels; the peroxisome cluster is indicated by a white arrow). Scale bar: 25 µm. A region at the cell periphery (blue box) and a region at the cell center (yellow box) are enlarged.

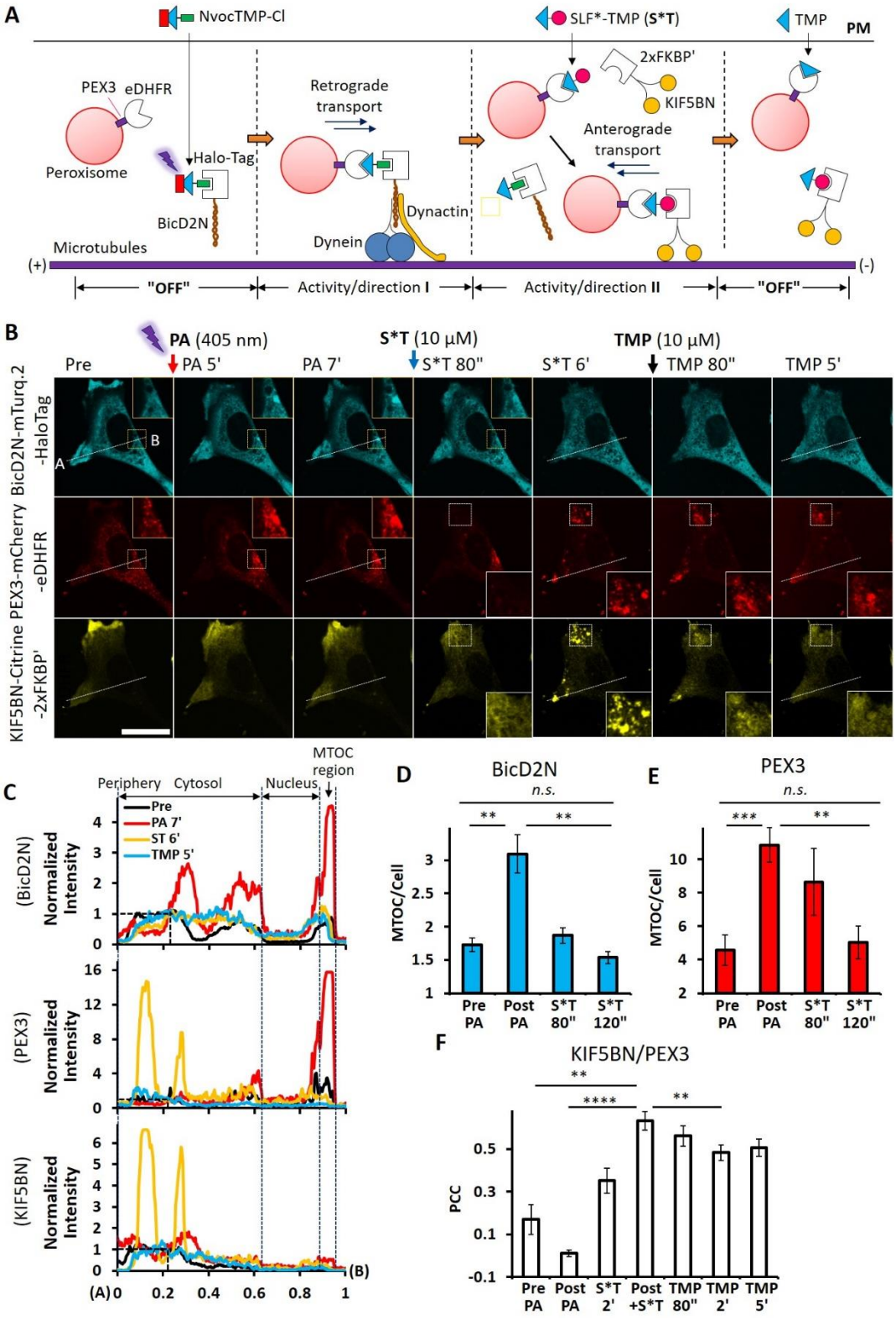

Figure S12. Competitive multi-directional activity control ("competitive MAC"). The cargo (peroxisome) was first transported to the center of a cell and then transported to the peripheral region of the cell, as

opposed to the experiment shown in Figure 2. **A**) Schematic representation of the experimental principle. **B**) Representative CLSM images of sequential recruitments of BicD2N and KIF5BN to peroxisomes, which induce the transport of peroxisomes to the cell center and cell periphery, respectively, followed by the displacement of motor proteins via the TMP competitor. Scale bar: 25 µm. A region at the cell center (yellow box) and a region at the cell periphery (white box) are enlarged. **C**) Line profile analysis of the CLSM images shown in B) before PA (Pre), 7 minutes after PA (PA 7'), 6 minutes after the addition of S*T (S*T 6'), and 5 minutes after adding TMP (TMP 5'). **D, E**) The fluorescence intensity ratio of BicD2N (D) or PEX3 (E) at the microtubule organization center (MTOC) versus in the entire cell increases after PA and decreases after adding S*T. This suggests that BicD2N is recruited to peroxisomes and induces retrograde transport of peroxisomes to the cell center upon photoactivation. S*T induces dissociation of BicD2N and recruitment of KIF5BN to peroxisomes, leading to anterograde transport of peroxisomes to the cell periphery. **F**) Pearson's correlation coefficient (PCC) analysis of the colocalization between KIF5BN-Citrine-eDHFR and PEX3-mCherry-HaloTag suggests that KIF5BN is recruited to peroxisomes after adding S*T and is dissociated from peroxisomes after the addition of TMP. Scale bar 25µm; for **D**), **E**), and **F**), error bars, SEM; n=6 cells from two independent experiments were analyzed; PEX3 indicates a peroxisome targeting peptide sequence; PA: photoactivation; p values are from paired Student's *t*-test (**: $p<0.01$, ***: $p<0.001$, ****: $p < 0.0001$; *n.s.*: non-significant); "Post PA" indicates 5-10 min after PA and just before adding S*T while "Post +S*T" means 5-10 min after the addition of S*T and just before adding TMP.

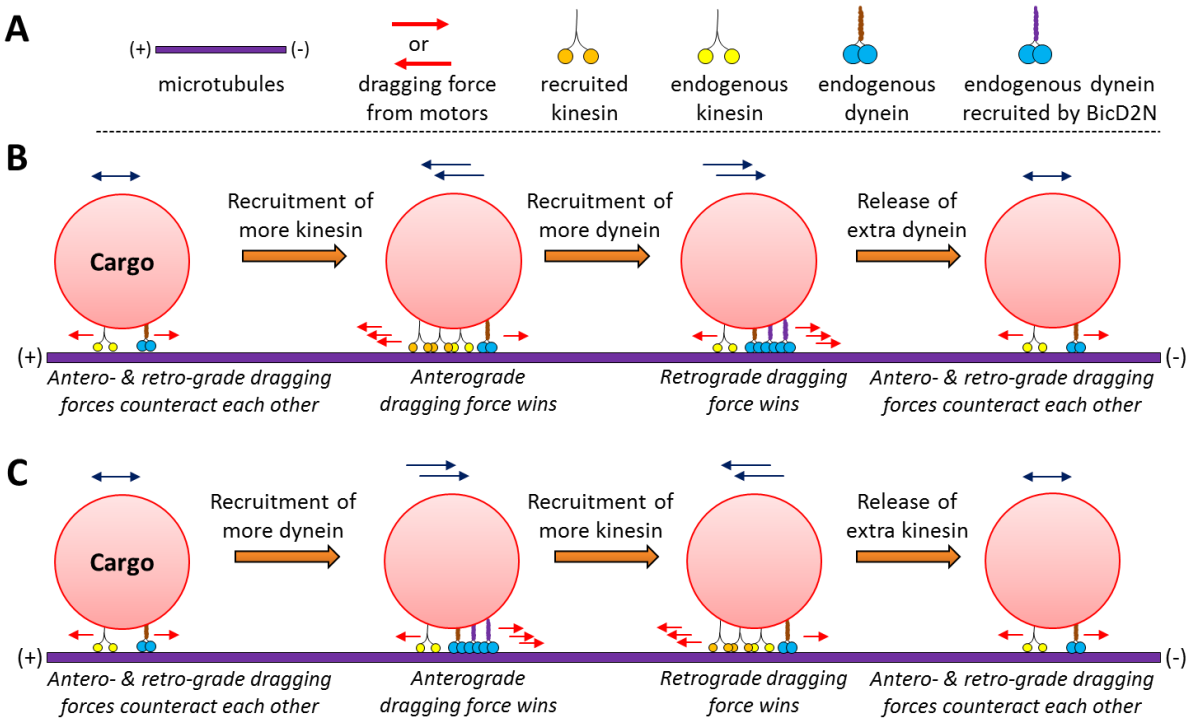

Figure S13. Our bidirectional peroxisome transport experiments support the "tug-of-war" model in bidirectional cargo transport. A) Denotations of symbols. **B**) Schematic representation of the "tug-of-war" model. An anterograde dragging force from endogenous kinesin and a retrograde dragging force from endogenous dynein counteract each other, which reduces net directional transport of cargos. Recruitment of extra kinesin motors leads to an imbalance; the anterograde dragging force becomes predominant and "wins", which leads to net cargo transport toward the plus end of microtubules. If dynein is recruited to the same cargo, for example, via exogenous regulators such as BicD2N, the retrograde dragging force "wins", leading to net cargo transport toward the minus end of microtubules. If the dynein and kinesin motor activities are again in balance after release of additional motors, net directional transport is reduced. In our experiments, we recapitulated these of events in an individual cell by directly controlling the dynein and kinesin activities on peroxisomes using the "competitive MAC" approach (Figure 3). This approach resulted in the expected net direction of cargo transport, which is thus in full agreement with the model of a dynein/kinesin-based "tug-of-war". **C**) The inversed bidirectional transport event, which corresponds to the scenario shown in Figure S12.

Supplementary Movie Legends

Movie S1: Parallel MAC. Before adding ST dimerizer, the overexpressed cytosolic Citrine-eDHFR-Rac1* caused significant background activity revealed by many membrane ruffles. The addition of ST dimerizer reduced the amount of ruffles, suggesting that the basal activity of Rac1* has been largely reduced. Finally local photoactivation at the rectangular area led to prominent local membrane ruffles formed only at the region of photoactivation (ROP).

Movie S2: Multi-directional activity control of Rac1 positioning. Rac1 was recruited to the plasma membrane after PA, translocated to the nucleus after adding S*T, and was rerouted back to the cytosol after adding TMP.

Movie S3: Competitive MAC where cargos were first transported to cell periphery then to cell center. NvocTMP-Cl was introduced onto HaloTag before experiment. Photoactivation led to the recruitment of KIF5BN onto peroxisomes, which stimulated anterograde transport of peroxisomes to the cell periphery (see white arrows). The addition of S*T led to the displacement of KIF5N by BicD2N, which promoted retrograde transport of peroxisomes to the cell center (see the white arrow). Final addition of TMP released BicD2N from peroxisomes and the overall processive movement of peroxisomes was stopped.

Movie S4: An enlarged region within the cell shows that the peroxisomes were first anterogradely transported to cell periphery after PA and then retrogradely transported toward the cell body after adding S*T.

Movie S5: Competitive MAC where cargos were first transported to the cell center then to the cell periphery. NvocTMP-Cl was introduced onto HaloTag before experiment. Photoactivation led to the recruitment of BicD2N onto peroxisomes, which induced retrograde transport of peroxisomes to the cell center. The addition of S*T led to the displacement of BicD2N by KIF5N, which triggered anterograde transport of peroxisomes to the cell periphery. Final addition of TMP released KIF5BN from peroxisomes and the overall possessive movement of peroxisomes was stopped.

ORGANIC SYNTHESIS

General

Unless otherwise specified, all chemicals were purchased from commercial sources and used without further purification. NMR spectra were measured on a Bruker AV400, or AV700 MHz magnetic resonance spectrometer. Data for ^{1}H-NMR and ^{13}C-NMR spectra are reported as follows: Chemical shifts are reported as δ in units of parts per million (ppm) relative to $CDCl_3$ (δ 7.26 for ^{1}H, δ 77 for ^{13}C); multiplicities are reported as follows: s (singlet), d (doublet), t (triplet), q (quartet), dd (doublet of doublets), m (multiplet), or br (broadened); coupling constants are reported as *J* values in Hertz (Hz); the number of protons (n) for a given resonance is indicated as nH, and is based on the spectra integration values. ESI-MS was performed on an Agilent 1100 series chromatography system equipped with an LCQ ESI mass spectrometer using C18 columns for small molecules. U-HPLC/MS are from Agilent Technologies (1290 Infinity) equipped with a DIONEX UltiMate 3000 Autosampler, DIONEX UltiMate 3000 Diode Array Detector, DIONEX Corona Veo RS Chareged Aerosal Detector, DIONEX Ultimate 3000 pump, DIONEX Ultimate 3000 Column Compartment, and a Quadrupole LC/MS (6150) module. Preparative HPLC-MS^{2} (Prep-MSII) is from Agilent Technologies equipped with a G1310B 1260 Iso Pump, G1361A 1260 PrepPump, and a Quadrupole LC/MS (6120) module. High resolution mass spectra (HRMS, 70 eV) were measured on a Thermo Orbitrap coupled to a Thermo Accela HPLC machine and using electron spray ionization technique (ESI) in positive mode unless otherwise noted.

Synthesis of SLF*-TMP (1) and key intermediates

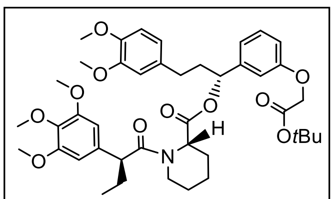

SLF'-COO*t*Bu (**4**)

(R)-1-(3-(2-(*tert*-butoxy)-2-oxoethoxy)phenyl)-3-(3,4-dimethoxyphenyl)propyl (S)-1-((S)-2-(3,4,5-trimethoxyphenyl)butanoyl)piperidine-2-carboxylate (SLF'-COO*t*Bu, **4**)**:** (R)-1-(3-(2-(*tert*-butoxy)-2-oxoethoxy)phenyl)-3-(3,4-dimethoxyphenyl)propyl (S)-piperidine-2-carboxylate (**2**) was prepared according to previously published[1]. Afterwards, the amine intermediate **2** (55 mg, 0.107 mol, M.W. 513), (S)-2-(3,4,5-trimethoxyphenyl)butanoic acid (**3**, 28.7 mg, 0.113 mmol, M.W. 254), EDC·HCl (30.7 mg, 0.16 mmol, M.W. 192) and HOBt·H_2O (24.5 mg, 0.16 mmol, M.W. 153) were dissolved in anhydrous DCM (2.14 ml, 0.05 M) followed by the injection of DIEA (35.9 mg, ~47.5µl, 0.278 mmol, M.W. 129). The reaction

mixture was stirred under N_2 at RT for 1 day until TLC (cyclohexane: EtOAc 1:1) revealed the fully conversion of SM to product. The reaction mixture was partitioned in EtOAc/aq. Na_2CO_3 (sat.) and the organic layer was separated. The aqueous phase was extracted twice more by EtOAc and all organic layers were combined, washed with brine, concentrated and dried over anhydrous Na_2SO_4. Silica gel chromatography purification yielded 46.7 mg SLF'-COO*t*Bu (**4**) as a light yellow sticky solid in a yield of 58%. **^{1}H-NMR** (400MHz, $CDCl_3$): δ 7.28 (m, 1H), 6.96 (m, 1H), 6.90 (m, 1H), 6.76-6.84 (m, 2H), 6.6-6.73 (m, 2H), 6.49 (s, 2H) <Ar-*H*, **9H**>; 5.77 (dd, J^1=7.7Hz, J^2=6.0Hz, 1H), 5.56 (d, J=4.76Hz, 1H), 4.52 (s, 2H), 3.83-3.87 (m, 12H), 3.70 (s, 3H), 3.60 (m, 2H), 3.11 (td, J^1=13.2Hz, J^2=2.76Hz, 1H) <-OCH_x-/=NCH_y-/-C(O)CH_z-, **22H**>; 2.54 (m, 2H), 2.25 (m, 2H), 2.08 (m, 2H), 1.92 (m, 1H), 1.79 (m, 1H), 1.69 (m, 2H), 1.57 (m, 2H), 1.49 (s, 9H), 0.91 (t, J=7.4Hz, 3H) <remained aliphatic *H*, **24H**>. **^{13}C-NMR** (101 MHz, $CDCl_3$): δ 172.60, 170.67, 167.82, 158.02, 153.25, 148.82, 147.27, 141.64, 136.80, 136.13, 133.45, 129.57, 120.08, 119.69, 113.79, 113.27, 111.67, 111.28, 104.79, 82.29, 75.99, 65.73, 60.79, 56.17, 56.85, 55.77, 52.10, 50.71, 43.31, 37.97, 31.13, 28.09, 27.97, 26.84, 24.80, 20.87, 12.49. **MS**(ESI), $C_{42}H_{56}NO_{11}^+$, calcd. 750.3848, found 750.11 $[M+H]^+$.

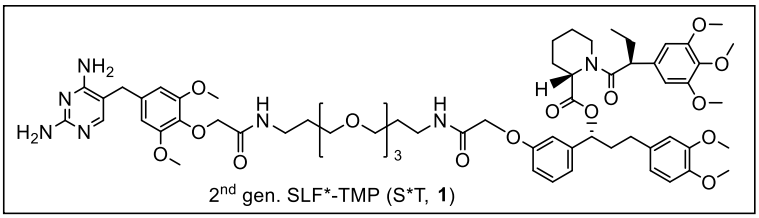

2nd gen. SLF*-TMP (S*T, **1**)

(R)-1-(3-((19-(4-((2,4-diaminopyrimidin-5-yl)methyl)-2,6-dimethoxyphenoxy)-2,18-dioxo-7,10,13-trioxa-3,17-diazanonadecyl)oxy)phenyl)-3-(3,4-dimethoxyphenyl)propyl (S)-1-((S)-2-(3,4,5-trimethoxyphenyl)butanoyl)piperidine-2-carboxylate (SLF*-TMP, i.e. S*T, **1**)**:** TMP-PEG_4-NH_2·xTFA was synthesized in 5 steps from trimethoprim (TMP, **5**) according to our previously published procedures[3, 5], and further purified via preparative HPLC [C18, 70% MeCN(0.1%TFA)/H_2O(0.1%TFA) isocratic elution, t_R 6.6min, λ=254 nm]. SLF'-COO*t*Bu (**4**, 46.7mg, 0.062 mol, M.W. 750) obtained from previous step was treated with 50% TFA/DCM at RT overnight, dried in vacuo, and silica gel chromatographed (1% HOAc in EtOAc) to afford the SLF'-COOH (*m/z* 694.4 $[M+H]^+$, M.W. 693) carboxylate intermediate. Afterwards, the purified SLF'-COOH, TMP-PEG_4-NH_2·xTFA (53.8 mg, M.W. 536+114x), HATU (44.3 mg, 0.116 mmol, M.W. 380) and HOBt·H_2O (13.6 mg, 0.089 mmol, M.W. 153) were dissolved in dry DMF (2.17 ml) followed by the injection of DIEA (34 mg, 45 µl, ~0.26 mmol, M.W. 129). The reaction mixture was stirred under N_2 at RT for 8 h to allow complete conversion of SLF'-COOH. The reaction mixture was diluted with EtOAc, washed with saturated $NaHCO_3$, brine, dried over anhydrous Na_2SO_4, filtered and concentrated under reduced

pressure. The residue was purified via reverse phase preparative HPLC-MS^2 [C18, 70% MeCN(0.1%TFA)/H_2O(0.1%TFA) isocratic elution, t_R 9.4min, λ=254 nm, *m/z* 606.5 $[M+2H]^{2+}$] to yield 16.7 mg light yellow solid as the SLF*-TMP (M.W. 1212) product in a yield of 22%. **^{1}H-NMR** (700MHz, $CDCl_3$): *δ* 8.78 (br, 2H),8.16 (m, 1H), 7.38 (m, 2H), 7.17 (t, *J*=8.0Hz, 1H), 7.00-6.96 (m, 1H), 6.96-6.86 (m, 1H), 6.86-6.74 (m, 4H), 6.74-6.57 (m, 3H), 6.46-6.38 (m, 3H) <Ar-*H* & -NH_x, **18H**>; 5.75-5.42 (m, 1H), 4.70-4.50 (m, 5H), 3.98-3.87 (m, 2H), 3.87-3.76 (m, 21H, -OCH_3), 3.76-3.59 (m, 5H), 3.59-3.50 (m, 10H), 3.47-3.17 (m, 4H) <=NCH_x-, -OCH_y-, -C(O)CH_z-, Ar-CH_2-Ar, **48H**>; 2.90-2.52 (m, 2H), 2.52-2.18 (m, 2H), 2.14-2.00 (m, 2H), 1.99-1.76 (m, 4H), 1.76-1.62 (m, 2H), 1.62-1.43 (m, 2H), 1.43-1.20 (m, 2H) <remained aliphatic *H*, **16H**>; 0.86 (t, *J*=7.35Hz, **3H**, -CH_2CH_3). **^{13}C-NMR** (176MHz, $CDCl_3$): *δ* 173.74, 171.50, 170.65, 169.43 <*C*=O, **4C**>; 164.13, 159.35, 159.12, 157.95, 157.19, 154.92, 153.36, 153.16, 152.82, 148.88, 147.39, 146.36, 142.08, 140.25, 136.91, 135.68, 134.22, 133.27, 131.18, 130.04, 129.68, 120.18, 119.39, 115.77, 114.15, 113.49, 112.41, 111.73, 111.27, 108.41, 105.36, 104.81 <Ar-*C*>; 76.26, 73.75, 71.79, 70.25, 70.08, 70.05, 69.34, 69.01, 66.94, 65.25 <O-*C*-, C(O)-*C*-N, **10C**>; 60.87, 56.22, 56.19, 55.91, 55.80 <-O*C*H_3, **5C** excluding 2 symmetric C>; 52.29, 50.71, 43.56, 40.46, 38.12, 37.16, 33.82, 31.55, 28.86, 27.72, 26.58, 24.71, 20.84, 12.34 <remained aliphatic *C*, **14C**>. **HPLC-MS** (C18, 10-100%MeCN/H_2O, λ=254nm): t_R=4.31min, *m/z* = 607.18 $[M+2H]^{2+}$, *m/z* = 1212.39 $[M+H]^+$. **HRMS**(ESI): $C_{63}H_{86}N_7O_{17}^+$, calcd. 1212.6075, found 1212.6072 $[M+H]^+$.

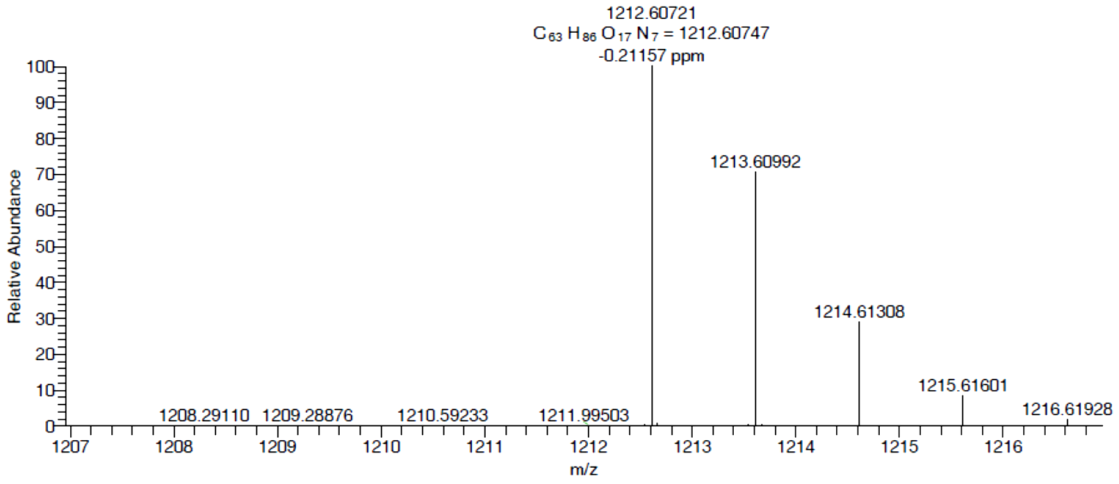

References:

1. Liu, P.; Calderon, A.; Konstantinidis, G.; Hou, J.; Voss, S.; Chen, X.; Li, F.; Banerjee, S.; Hoffmann, J. E.; Theiss, C.; Dehmelt, L.; Wu, Y. W., A Bioorthogonal Small-Molecule-Switch System for Controlling Protein Function in Live Cells. *Angew. Chem. Int. Edit.* **2014,** *53* (38), 10049-10055.
2. Chen, X.; Venkatachalapathy, M.; Kamps, D.; Weigel, S.; Kumar, R.; Orlich, M.; Garrecht, R.; Hirtz, M.; Niemeyer, C. M.; Wu, Y.-W.; Dehmelt, L., "Molecular-Activity Painting": Switch-like, Light-Controlled Perturbations inside Living Cells. *Angew. Chem. Int. Edit.* **2017,** *56*, 5196-5920.
3. Chen, X.; Li, F.; Wu, Y. W., Chemical labeling of intracellular proteins via affinity conjugation and strain-promoted cycloadditions in live cells. *Chem. Commun.* **2015,** *51* (92), 16537-40.
4. Bentley, M.; Decker, H.; Luisi, J.; Banker, G., A novel assay reveals preferential binding between Rabs, kinesins, and specific endosomal subpopulations. *J. Cell Biol.* **2015,** *208* (3), 273-281.
5. Liu, W.; Li, F.; Chen, X.; Hou, J.; Yi, L.; Wu, Y. W., A Rapid and Fluorogenic IMP-AcBODIPY Probe for Covalent Labeling of Proteins in Live Cells. *J. Am. Chem. Soc.* **2014,** *136* (12), 4468-4471.

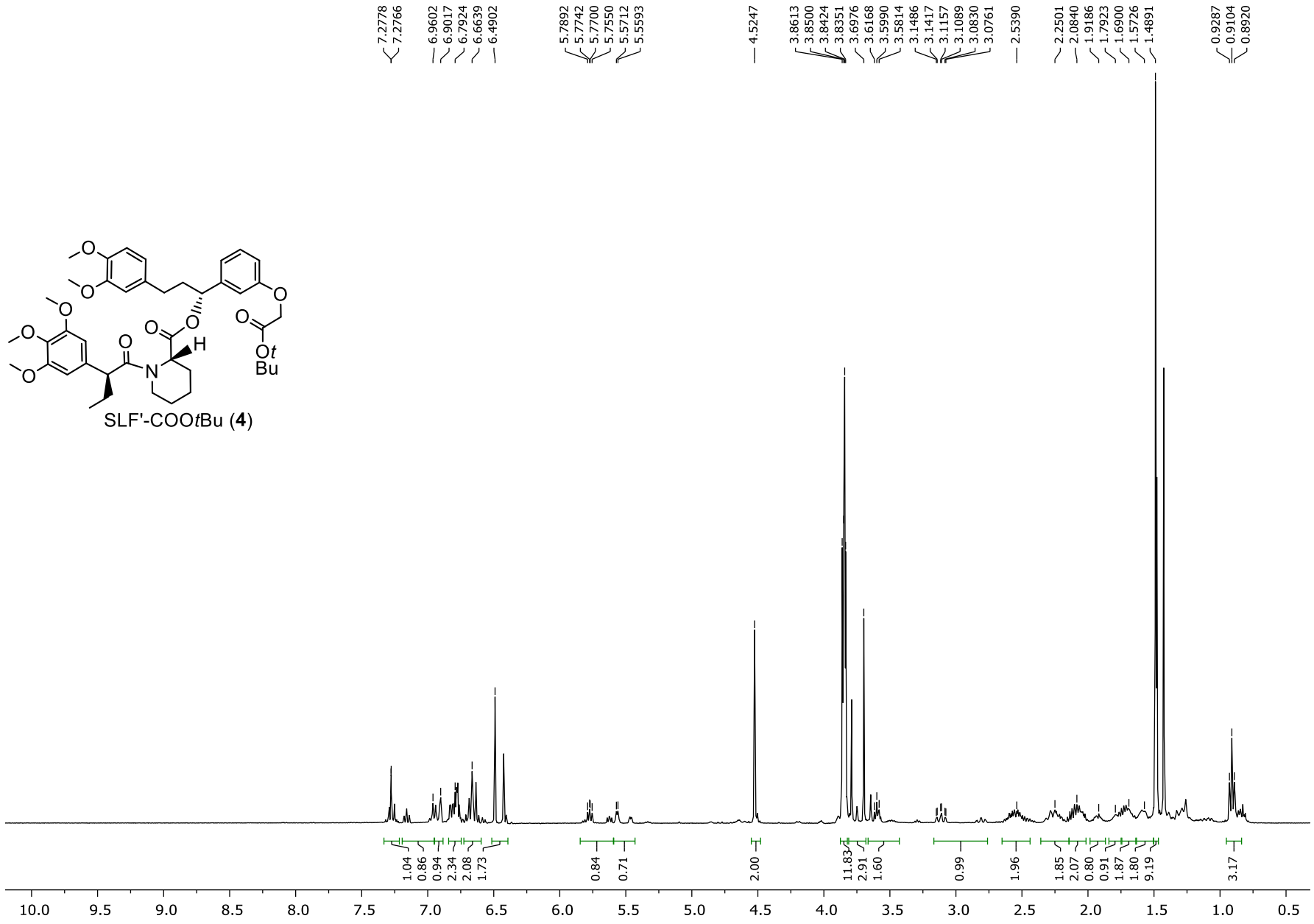
7.2778
7.2766
6.9602
6.9017
6.7924
6.6639
6.4902
5.7892
5.7742
5.7700
5.7550
5.5712
5.5593
4.5247
3.8613
3.8500
3.8424
3.8351
3.6976
3.6168
3.5990
3.5814
3.1486
3.1417
3.1157
3.1089
3.0830
3.0761
2.5390
2.2501
2.0840
1.9186
1.7923
1.6900
1.5726
1.4891
0.9287
0.9104
0.8920
1.04
0.86
0.94
2.34
2.08
1.73
0.84
0.71
2.00
11.83
2.91
1.60
0.99
1.96
1.85
2.07
0.80
0.91
1.87
1.80
9.19
3.17
10.0
9.5
9.0
8.5
8.0
7.5
7.0
6.5
6.0
5.5
5.0
4.5
4.0
3.5
3.0
2.5
2.0
1.5
1.0
0.5

SLF'-COO*t*Bu (**4**)

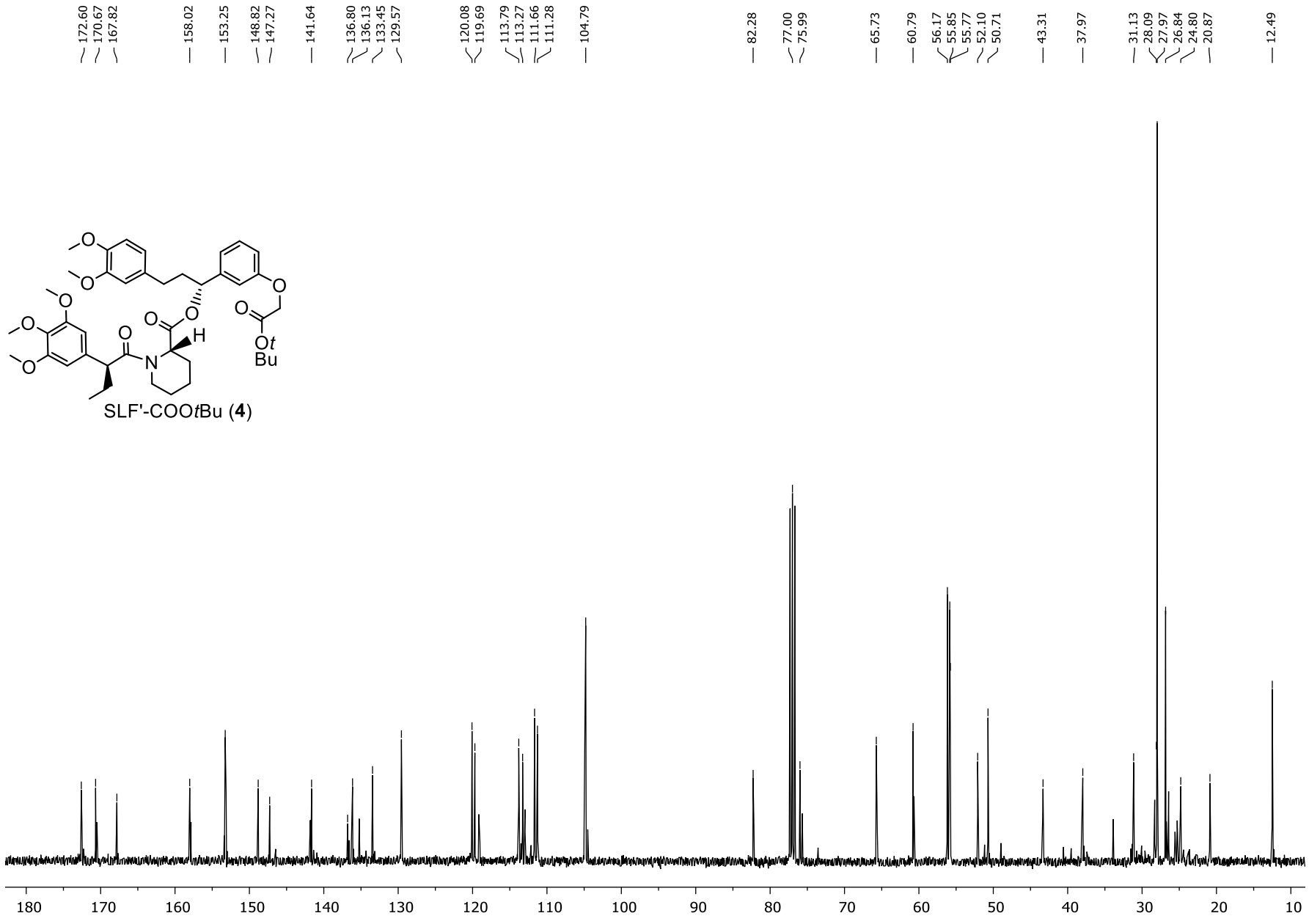
172.60
170.67
167.82
158.02
153.25
148.82
147.27
141.64
136.80
136.13
133.45
129.57
120.08
119.69
113.79
113.27
111.66
111.28
104.79
82.28
77.00
75.99
65.73
60.79
56.17
55.85
55.77
52.10
50.71
43.31
37.97
31.13
28.09
27.97
26.84
24.80
20.87
12.49
SLF'-COO*t*Bu (**4**)
180
170
160
150
140
130
120
110
100
90
80
70
60
50
40
30
20
10

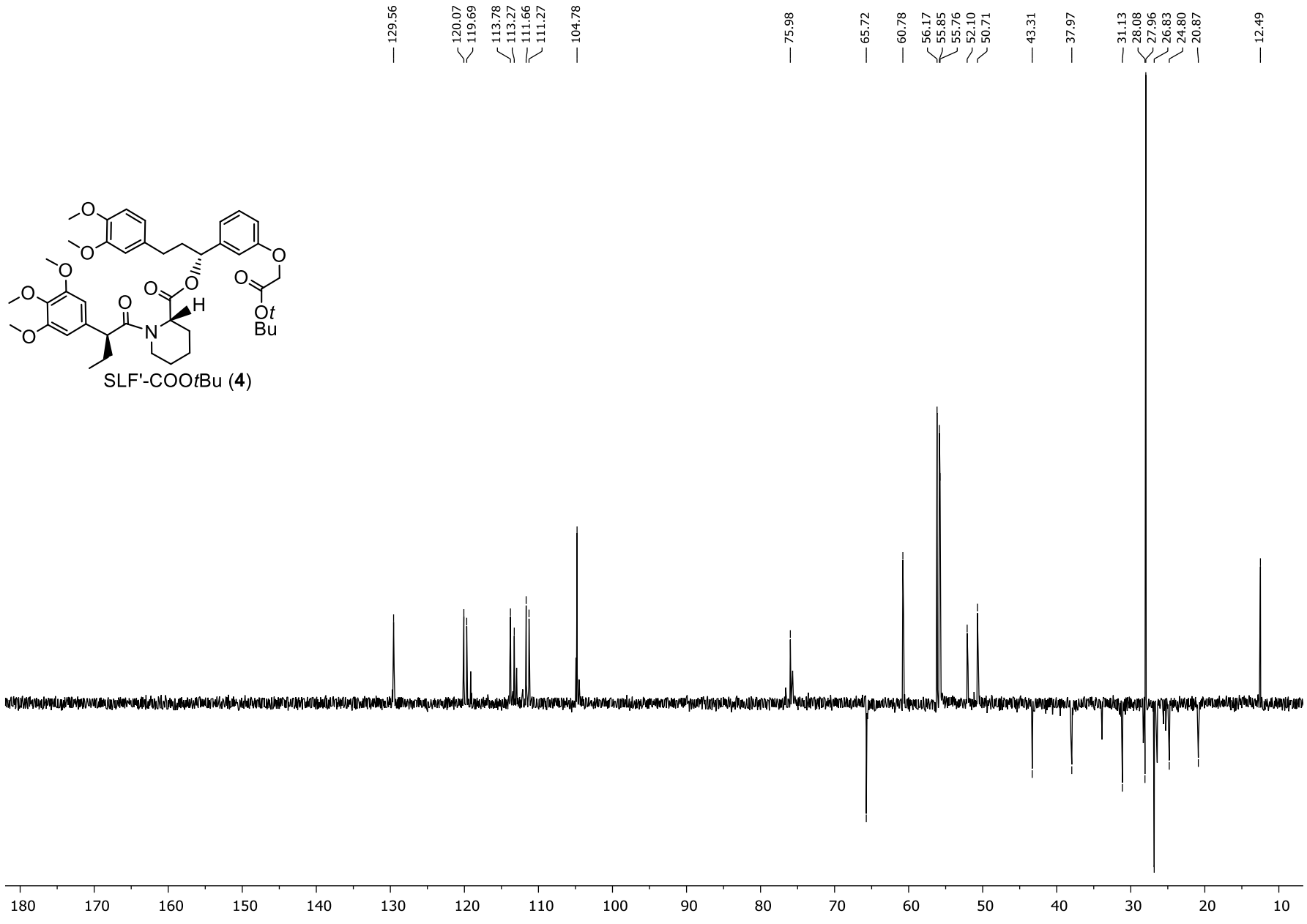
129.56
120.07
119.69
113.78
113.27
111.66
111.27
104.78
75.98
65.72
60.78
56.17
55.85
55.76
52.10
50.71
43.31
37.97
31.13
28.08
27.96
26.83
24.80
20.87
12.49
SLF'-COO*t*Bu (**4**)
180
170
160
150
140
130
120
110
100
90
80
70
60
50
40
30
20
10

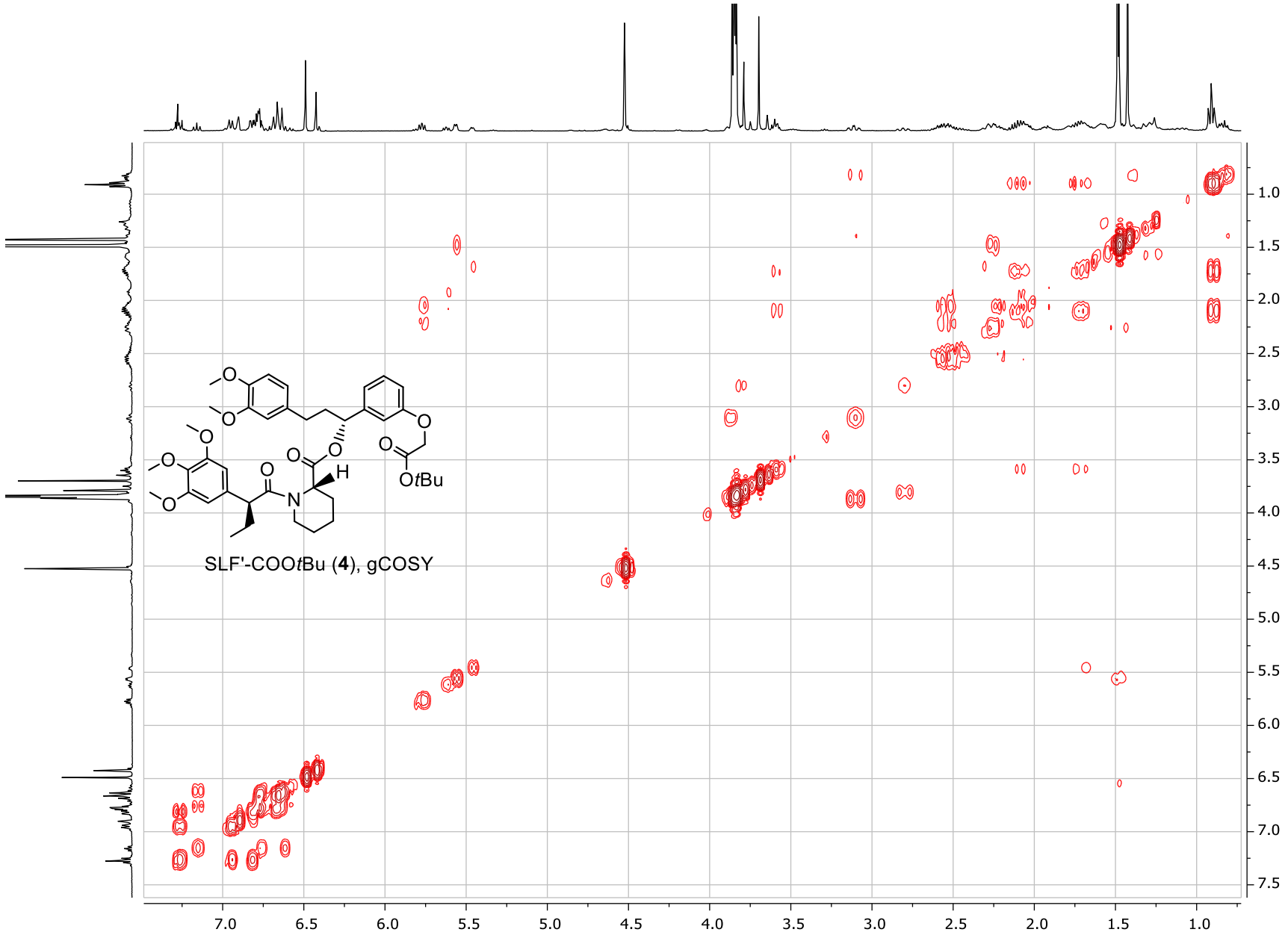
SLF'-COO*t*Bu (**4**), gCOSY
OtBu
7.0
6.5
6.0
5.5
5.0
4.5
4.0
3.5
3.0
2.5
2.0
1.5
1.0
7.5

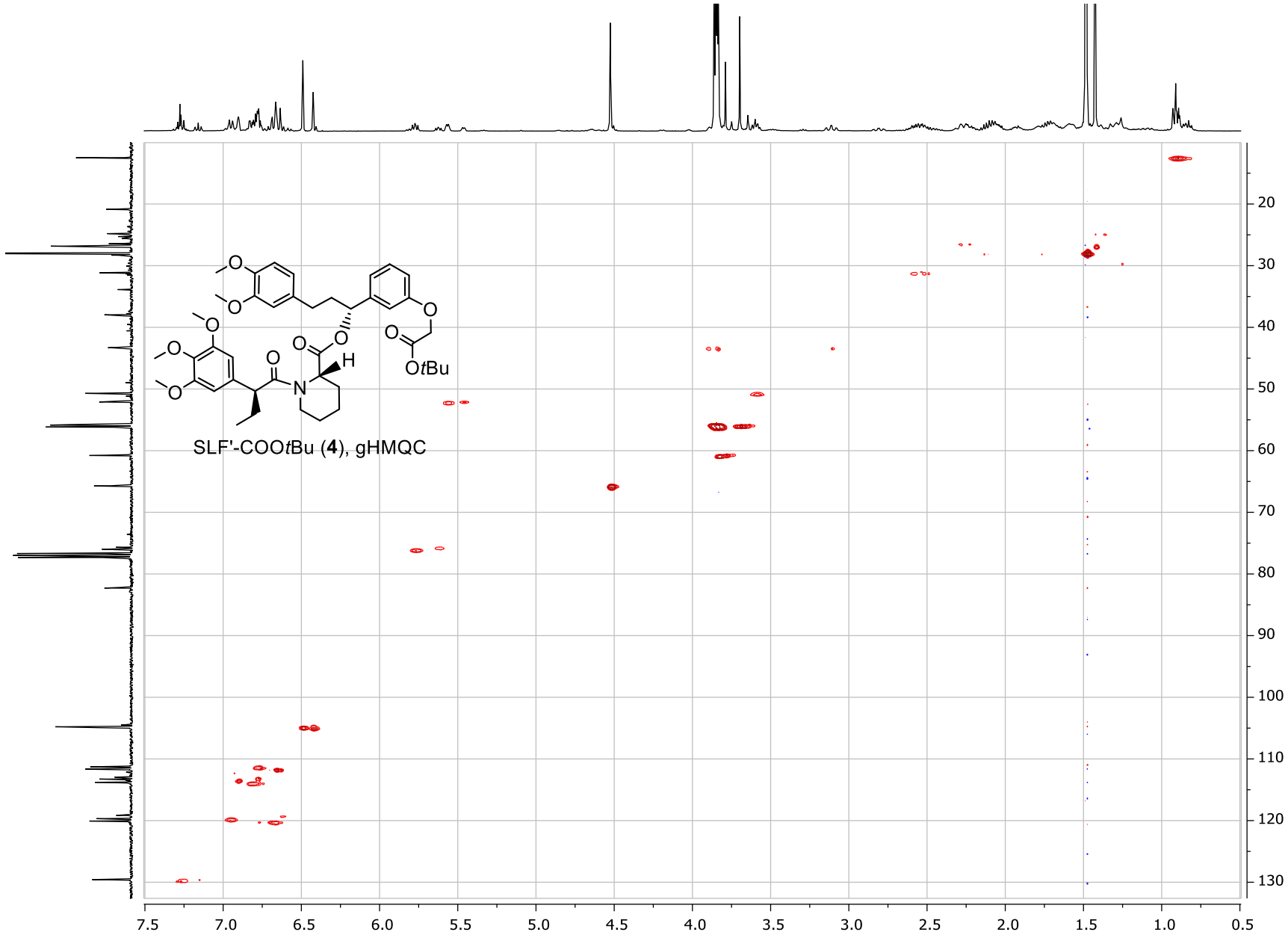
SLF'-COO*t*Bu (**4**), gHMQC
OtBu
7.5
7.0
6.5
6.0
5.5
5.0
4.5
4.0
3.5
3.0
2.5
2.0
1.5
1.0
0.5
20
30
40
50
60
70
80
90
100
110
120
130

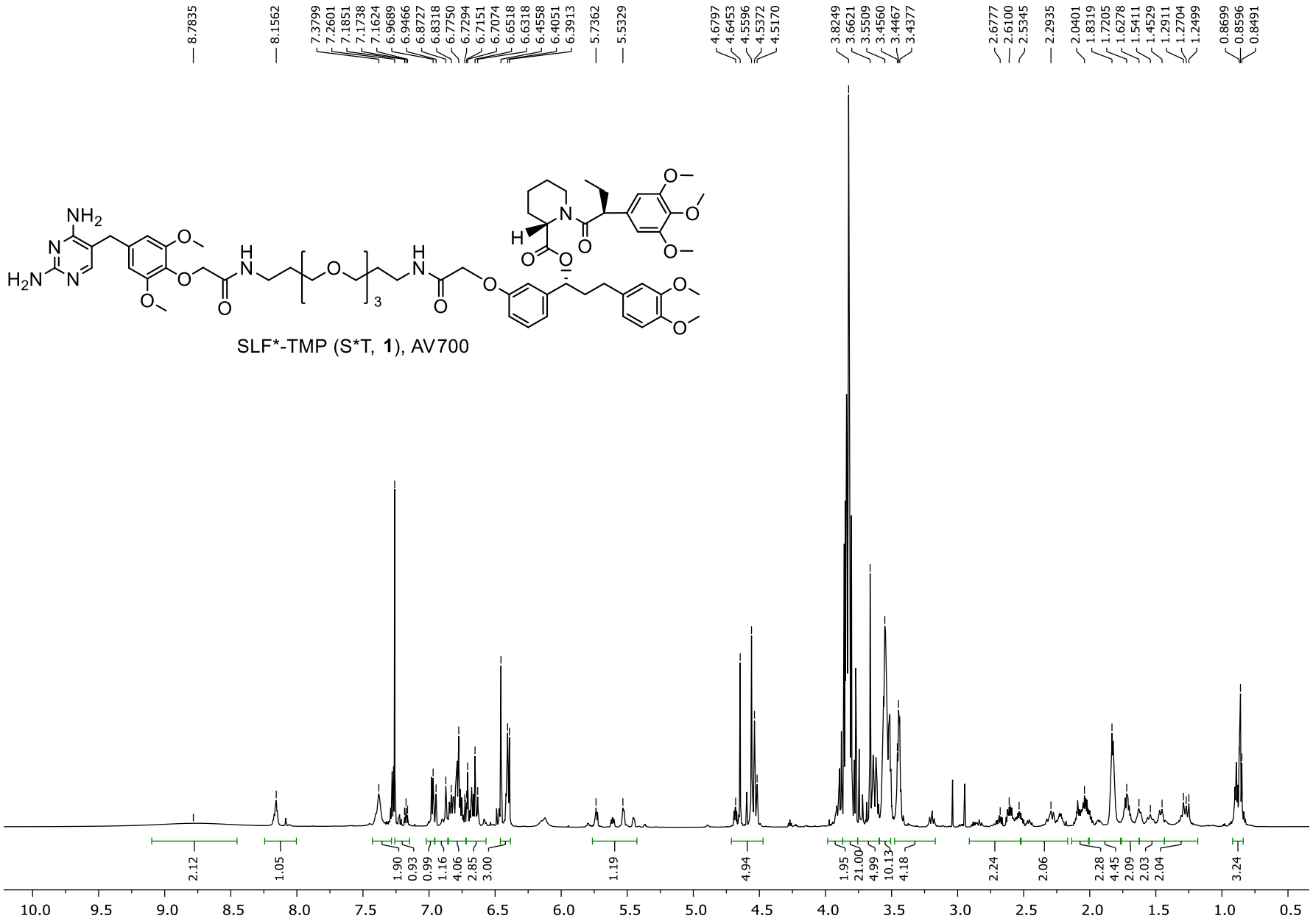
8.7835
8.1562
7.3799
7.2601
7.1851
7.1738
7.1624
6.9689
6.9466
6.8727
6.8318
6.7750
6.7294
6.7151
6.7074
6.6518
6.6318
6.4558
6.4051
6.3913
5.7362
5.5329
4.6797
4.6453
4.5596
4.5372
4.5170
3.8249
3.6621
3.5509
3.4560
3.4467
3.4377
2.6777
2.6100
2.5345
2.2935
2.0401
1.8319
1.7205
1.6278
1.5411
1.4529
1.2911
1.2704
1.2499
0.8699
0.8596
0.8491
SLF*-TMP (S*T, 1), AV700
2.12
1.05
1.90
0.93
0.99
1.16
4.06
2.85
3.00
1.19
4.94
1.95
21.00
4.99
10.13
4.18
2.24
2.06
2.28
4.45
2.09
2.03
2.04
3.24
10.0
9.5
9.0
8.5
8.0
7.5
7.0
6.5
6.0
5.5
5.0
4.5
4.0
3.5
3.0
2.5
2.0
1.5
1.0
0.5

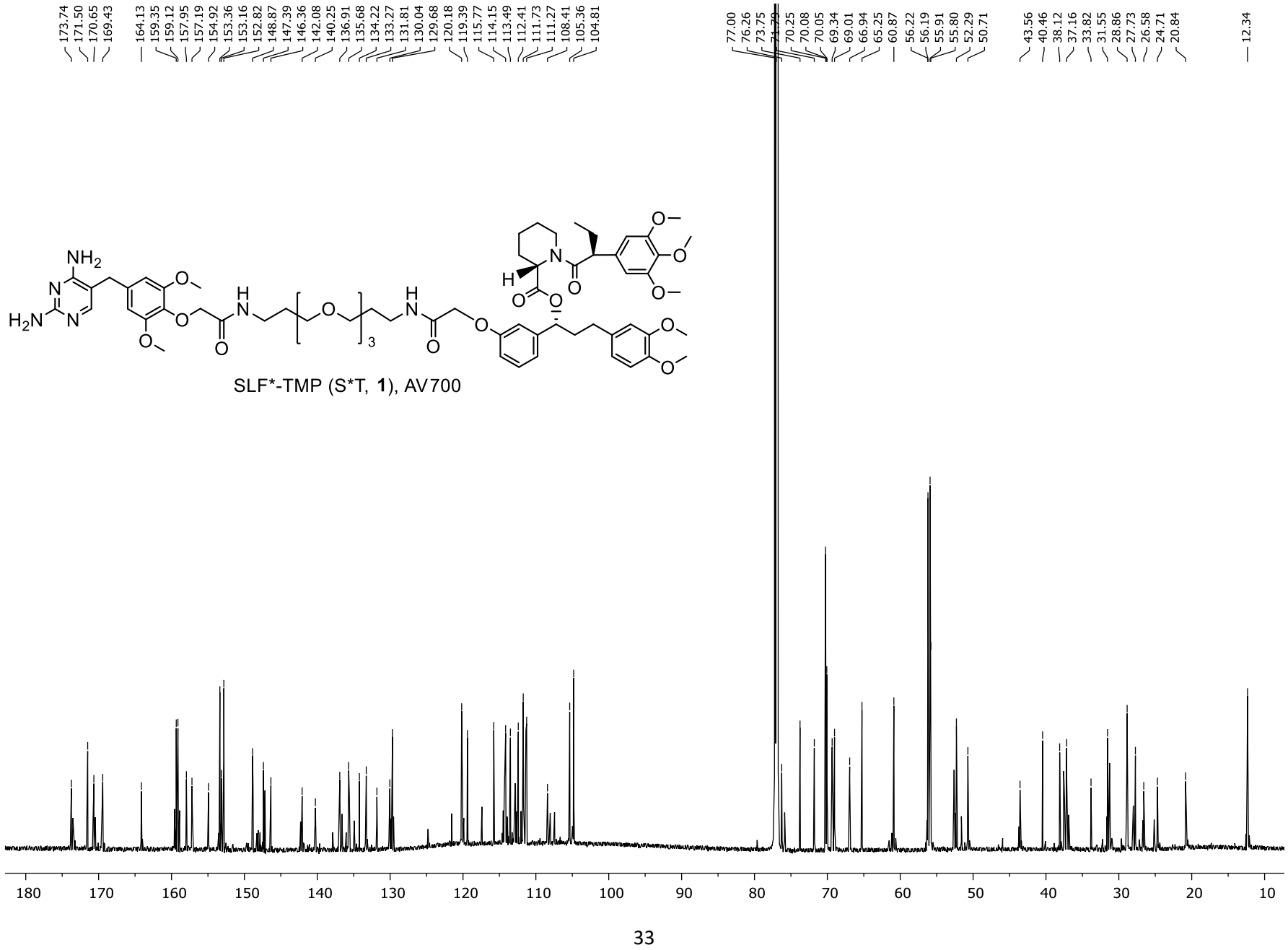
173.74
171.50
170.65
169.43
164.13
159.35
159.12
157.95
157.19
154.92
153.36
153.16
152.82
148.87
147.39
146.36
142.08
140.25
136.91
135.68
134.22
133.27
131.81
130.04
129.68
120.18
119.39
115.77
114.15
113.49
112.41
111.73
111.27
108.41
105.36
104.81
77.00
76.26
73.75
71.79
70.25
70.08
70.05
69.34
69.01
66.94
65.25
60.87
56.22
56.19
55.91
55.80
52.29
50.71
43.56
40.46
38.12
37.16
33.82
31.55
28.86
27.73
26.58
24.71
20.84
12.34
SLF*-TMP (S*T, 1), AV700
180
170
160
150
140
130
120
110
100
90
80
70
60
50
40
30
20
10